

## Drivers of Interannual Salinity Variability in the Arctic Ocean

 Antoine Hochet<sup>1</sup> , Camille Lique<sup>1</sup> , Florian Sévellec<sup>1,2</sup>, and William Llovel<sup>1</sup> 
<sup>1</sup>Laboratoire d'Océanographie Physique et Spatiale, University Brest CNRS IRD Ifremer, Brest, France, <sup>2</sup>Odyssey Team-project, INRIA CNRS, Paris, France

**Special Collection:**

The Arctic Ocean's changing Beaufort Gyre

**Key Points:**

- A novel diagnostic is developed allowing the analysis of the mechanisms of salinity variability in realistic configurations of the Arctic
- The main source of Arctic interannual salinity variability is associated to wind forcing variations, the main sink to mesoscale eddies
- Diffusion and freshwater fluxes (mainly due to sea-ice melt and freeze) play a non-negligible role, particularly over the continental shelf

**Correspondence to:**

 A. Hochet,  
antoine.hochet@univ-brest.fr

**Citation:**

 Hochet, A., Lique, C., Sévellec, F., & Llovel, W. (2024). Drivers of interannual salinity variability in the Arctic Ocean. *Journal of Geophysical Research: Oceans*, 129, e2023JC020852. <https://doi.org/10.1029/2023JC020852>

Received 21 DEC 2023

Accepted 26 APR 2024

**Author Contributions:**
**Conceptualization:** Antoine Hochet, Camille Lique, Florian Sévellec, William Llovel

**Investigation:** Antoine Hochet

**Methodology:** Antoine Hochet, Camille Lique, Florian Sévellec, William Llovel

**Validation:** Antoine Hochet

**Writing – original draft:** Antoine Hochet

**Writing – review & editing:**

Antoine Hochet, Camille Lique, Florian Sévellec, William Llovel

© 2024 The Authors.

 This is an open access article under the terms of the [Creative Commons Attribution-NonCommercial License](#), which permits use, distribution and reproduction in any medium, provided the original work is properly cited and is not used for commercial purposes.

**Abstract** Accurate projections and attribution of Arctic Ocean changes in climate models require a good understanding of the mechanisms underlying interannual salinity variability in the region. Although some mechanisms have been extensively studied in idealized setting, in particular for the dynamics of the Beaufort gyre (BG), it remains unclear how applicable they are to more complex systems. This study introduces a new diagnostic based on salinity variance budget to robustly assess the mechanisms of salinity variations. The diagnostic is then applied to the “Estimating the Circulation and Climate of the Ocean” state estimate. Results indicate that the advection of salinity anomaly in the direction of the mean salinity gradient made by velocity anomalies is the primary source of interannual salinity variability. These velocities are primarily attributed to fluctuating winds via Ekman transports. Fluctuating surface freshwater fluxes from the atmosphere and sea ice are the second most important source of variability and cannot be neglected. The two sinks of interannual salinity variance are associated with the erosion of large scale gradients of the mean circulation by eddies and to a lesser extent to the diffusive terms. Over continental shelves, particularly over the East Siberian Shelf (ESS), ocean surface freshwater fluxes and diffusion play a more important role than in the deep basins. We also report a strong intensification of all sources and sinks of interannual salinity variability in the BG and an opposite weakening in the ESS in the second decade of the analysis (2004–2014) with respect to the first (1993–2003).

**Plain Language Summary** A clear understanding of the mechanisms of the slow salinity variations in the Arctic could help improving their representation in climate models and provide directions on where new in-situ observing systems should be positioned. Most of the past studies of the mechanisms have used simple models in which several important realistic characteristics, such as the true bathymetry, are missing. In this work we develop a novel methodology that allows to robustly assess these mechanisms in realistic configurations. We then apply this methodology to an ocean state estimate (“Estimating the Circulation and Climate of the Ocean” v4r3) and study in details the forcing and damping mechanisms of the salinity variability in the Arctic. We find that the fluctuating wind is the main driver of the variability whereas mesoscale eddies are the main damping. Varying freshwater fluxes and diffusion also play a role and cannot be neglected.

### 1. Introduction

Salinity plays a crucial role for the Arctic Ocean dynamics. The density of the Arctic is mainly controlled by salinity rather than temperature (Aagaard & Carmack, 1989), and fresh waters overlies saltier waters. This salinity stratification is essential for the presence of sea ice because it acts to inhibit deep thermal convection (Bulgakov, 1962; Carmack, 2007; Timmermans & Marshall, 2020) and insulates Arctic sea ice from the warmer Pacific- and Atlantic-origin water masses at depth. Moreover, the variations in Arctic freshwater content are also believed to impact other regions via the export of freshwater to the North Atlantic. This export has been suggested to influence the stratification in the deep convection region and to modify the intensity of the Atlantic Meridional Overturning Circulation (Jahn & Holland, 2013; Karcher et al., 2005; Sévellec & Fedorov, 2016; H. Wang et al., 2018). Therefore, understanding the mechanisms at the origin of the salinity variations in the Arctic is of great interest. Moreover climate models are known to have important biases in their representation of sea ice and salinity (Khosravi et al., 2022; Notz & Community, 2020; Shu et al., 2020). A clear understanding of the mechanisms at play for the past salinity variations and a comparison with their representation in climate models could provide important directions on how to tackle model's deficiencies in the Arctic.

The mean freshwater balance of the Arctic Ocean has been studied by many authors (e.g., Häkkinen & Proshutinsky, 2004; Holland et al., 2006; Jahn et al., 2012; Johnson et al., 2018; Köberle & Gerdes, 2007; Lique

et al., 2009; Serreze et al., 2006; Steele et al., 1997; Tsubouchi et al., 2018; Wang et al., 2016). The main freshwater sources are the river discharge, the inflow of relatively fresh water through Bering Strait and the net precipitation, while the main sink is associated to the export of liquid freshwater and sea ice to the North Atlantic through the Canadian Arctic Archipelago and through Fram Strait (Serreze et al., 2006). Although the Arctic Ocean is small in terms of volume (1%), it is an important region of freshwater input to the world oceans as it receives approximately 11% of all rivers discharge (Aagaard & Carmack, 1989; Dai & Trenberth, 2002; Timmermans & Marshall, 2020). The Arctic freshwater content interannual and longer variability is mainly due to the variability of the advective exchanges with the North Atlantic, and with the North Pacific (Lique et al., 2009). The Arctic freshwater balance allows to understand the respective role of the advective flux to/from the bordering sub Arctic Oceans. However, because of the volume integral over the Arctic Ocean used in this methodology, local effects, within the Arctic Ocean, are difficult to isolate. Fluctuating spatial redistribution of the Arctic salinity field may indeed happen without any change in its global freshwater content (Lique et al., 2011; Morison et al., 2012).

The major component of the freshwater content variability in the Arctic is associated to the Beaufort Gyre (BG) (Haine et al., 2015; Stewart & Haine, 2013). The BG is a large scale oceanic circulation driven by anticyclonic winds associated with the Beaufort Sea High pressure system (Aagaard & Carmack, 1989). Anticyclonic winds result in the convergence of freshwater toward the center of the BG where it down wells due to Ekman pumping (Proshutinsky et al., 2002). Interannual variations in the BG freshwater content are associated with strong modification of the overlying wind regime: stronger than normal anticyclonic conditions leads to increased BG freshwater content, while cyclonic regime implies a decrease in BG freshwater content (Proshutinsky et al., 2002). More recently, it has been shown that eddies also play an important role in controlling the variability (Davis et al., 2014; Manucharyan et al., 2016; Manucharyan & Spall, 2016; Meneghello et al., 2017; Yang et al., 2016). Using the residual mean circulation framework, Manucharyan et al. (2016) show that the halocline depth variations in the BG are controlled by a competition between oceanic mesoscale eddies and Ekman pumping via wind variations. The effect of sea ice has also been suggested to play an important role in controlling the BG balance through a mechanism that has been named the “ice-ocean stress governor” (Doddrige et al., 2019; Meneghello et al., 2018), that tends to modulate strongly (or even turn off) the intensity of the surface Ekman pumping. Because these studies of the BG mechanisms have been mostly performed using idealized simple models in which authors assume flat bottom topography, idealized wind stress and freshwater forcing, how these theories apply concretely to a realistic BG remains unclear.

In particular, what is the relative importance of the wind forcing and buoyancy flux forcing in setting these variations? Adiabatic eddy-induced advection is suggested to balance the downwelling due to wind in the BG (Manucharyan et al., 2016), but it is unclear if this mechanism is important elsewhere in the Arctic, and what is the role and importance of the diffusive terms associated to diabatic processes in controlling the variability. Moreover, most of the previous studies have only focused on freshwater storage in the BG, however, the shelves (such as the East Siberian Shelf—ESS) may also contribute to the Arctic freshwater storage (see for instance Figure 1 in Johnson et al., 2018) and it is thus important to extend the study of salinity variations to the whole Arctic basin.

To address these points, we use here a new framework based on salinity variance budgets that allows to compute the local sources and sinks of interannual variability of salinity in realistic configurations and thus to understand the mechanisms at play for its variability. Similar density variance budgets have been widely used in previous studies to study the mechanisms of the Atlantic Multidecadal Variability (AMV) in idealized configuration of the North Atlantic (Arzel et al., 2006; Colin de Verdière & Huck, 1999) as well as in realistic configurations (Arzel et al., 2018; Gastineau et al., 2018). It has also been applied to study the interaction between meso-scale turbulence and the AMV for the ocean temperature (Hochet et al., 2020) or to disentangle the role of eddies in setting buoyancy variance in the Southern Ocean using 2-year long mooring observations (Sévellec et al., 2021). Recently this diagnostic has proved useful to understand the mechanisms of steric sea level interannual and seasonal variability (Hochet et al., 2023, 2024). Here, we derive a similar variance budget for the salinity and apply this budget to the Estimating the Circulation and Climate of the Ocean (ECCO) v4r3 state estimate (Forget et al., 2015).

The remainder of this article is organized as follows: in Section 2 we derive the salinity variance budget and in Section 3, we present the ECCO v4r3 state estimate. In Section 4.1, we compute and discuss the different terms of the Arctic salinity variance budget obtained from ECCO over the period 1993–2014, in Section 4.2 we decompose the oceanic advective term into different components associated to different physical mechanisms, in Section 4.3

we assess the effect of wind variability on the salinity variations, and in Section 4.4, we relate our methodology to previous work based on the residual mean framework. In Section 5, we show how the salinity variance budget underwent significant changes in the last years of the study period. Finally, in Section 6 we summarize and discuss our main results.

## 2. Method: Interannual Salinity Variance Budget

### 2.1. Decomposition Into Advection, Diffusion and Freshwater Flux Terms

Each variable  $X$  is decomposed into their time mean  $\langle \cdot \rangle$ , interannual, and sub-annual parts:

$$X = \bar{X} + X' + X^{\text{sub}}, \quad (1)$$

where  $X'$  and  $X^{\text{sub}}$  stand respectively for the interannual and sub-annual parts of  $X$  and are obtained by means of the low pass filter  $\langle \cdot \rangle$  (i.e.,  $X' = \langle X - \bar{X} \rangle$  and  $\langle X^{\text{sub}} \rangle = 0$ ).

The evolution equation for the interannual salinity variations can be decomposed as:

$$\frac{\partial S'}{\partial t} = \text{adv}' + \text{dif}' + \text{flu}', \quad (2)$$

where  $S'$  is the interannual salinity anomaly,  $\text{adv}'$  is the effect of advective terms,  $\text{dif}'$  is the effect of diffusive terms, and  $\text{flu}'$  is the effect of the surface freshwater fluxes from evaporation, precipitation, river run-off, and sea ice melt and freezing. The time average of the product of Equation 2 with  $S'$  gives the local interannual salinity variance budget.

$$\frac{1}{2} \frac{\partial \overline{(S')^2}}{\partial t} = \overline{S' \text{adv}'} + \overline{S' \text{dif}'} + \overline{S' \text{flu}'}, \quad (3)$$

$$\text{RES} = \text{VAR}_{\text{adv}} + \text{VAR}_{\text{dif}} + \text{VAR}_{\text{flu}}. \quad (4)$$

When one of the three terms in the right hand side of Equation 3 is positive (negative) then it is a source (sink) of interannual salinity variance. By examining the sign and relative intensity of the interannual salinity variance terms, it is then possible to determine which term is locally driving or damping the interannual variations of salinity. For instance,  $\text{VAR}_{\text{flu}} = \overline{S' \text{flu}'}$  can be a source in two cases: (a) if  $S' > 0$  and  $\text{flu}' > 0$  because  $\text{flu}'$  acts to increase the positive anomaly of  $S'$  or (b) if  $S' < 0$  and  $\text{flu}' < 0$  because  $\text{flu}'$  acts to decrease the negative anomaly of  $S'$ . The sum of the three terms in the right hand side of Equation 3 is equal to the time variations of the interannual salinity variance. In a statistical steady state, this residual term (RES) is zero and the three right hand side terms must balance. It follows that if one of the three terms is non-zero, there must be at least one other non-zero term of opposite sign to achieve a balance.

### 2.2. Decomposition of the Advective Term

The advective term  $\text{VAR}_{\text{adv}} = \overline{S' \text{adv}'}$  in Equation 3 can be decomposed as the sum of different terms arising from different dynamical features. Using the time scale decomposition given by Equation 1, the advective term from the salinity evolution equation  $\text{adv}'$  can be decomposed as:

$$\text{adv}' = \underbrace{-\nabla \cdot \mathbf{V} S'}_{\text{adv}'_{\text{adv}}} - \underbrace{\nabla \cdot \mathbf{v}' \bar{S}}_{\text{adv}'_{\text{mean}}} - \underbrace{\nabla \cdot \mathbf{v}'_{\text{GM}} \bar{S}}_{\text{adv}'_{\text{eddy}}} - \nabla \cdot (\mathbf{v}' S' - \mathbf{v}'_{\text{GM}} S') + \text{adv}'_{\text{sub}}, \quad (5)$$

where  $\mathbf{V}$  is the sum of the time mean and interannual velocities and the time mean and interannual GM eddy-induced velocities (i.e.,  $\mathbf{V} = \bar{\mathbf{v}} + \mathbf{v}' + \bar{\mathbf{v}}_{\text{GM}} + \mathbf{v}'_{\text{GM}}$ ),  $\text{adv}'_{\text{adv}}$  is the advection of salinity anomalies by  $\mathbf{V}$ ,  $\text{adv}'_{\text{mean}}$  is the advection of mean salinity by velocity interannual anomalies,  $\text{adv}'_{\text{eddy}}$  is the advection of the mean salinity by the interannual anomalies of GM parametrized eddy-induced velocity, and  $\text{adv}'_{\text{sub}}$  represents the effect

of all sub-annual frequencies and is obtained as a residual. Then, the time average of the product between Equation 5 and  $S'$  gives the following decomposition of the advective term for the salinity variance budget:

$$\begin{aligned} \text{VAR}_{\text{adv}} &= \overline{S' \text{adv}'_{\text{adv}}} + \overline{S' \text{adv}'_{\text{mean}}} + \overline{S' \text{adv}'_{\text{eddy}}} + \overline{S' \text{adv}'_{\text{sub}}}, \\ &= \underbrace{-\nabla \cdot \mathbf{v} \frac{(S')^2}{2}}_{\text{VAR}_{\text{adv}}^{\text{adv}}} + \underbrace{\overline{\mathbf{v}' S' \cdot \nabla \bar{S}}}_{\text{VAR}_{\text{adv}}^{\text{mean}}} - \underbrace{\overline{\mathbf{v}'_{\text{GM}} S' \cdot \nabla \bar{S}}}_{\text{VAR}_{\text{adv}}^{\text{eddy}}} + \underbrace{\overline{S' \text{adv}'_{\text{sub}}}}_{\text{VAR}_{\text{adv}}^{\text{sub}}}. \end{aligned} \quad (6)$$

$\text{VAR}_{\text{adv}}^{\text{adv}}$  is the local convergence of the interannual salinity variance resulting from both the mean velocity and eddy-induced velocity. This term is the advection of the salinity variance and can only redistribute salinity variance, but cannot act as a net source or sink of salinity variance.  $\text{VAR}_{\text{adv}}^{\text{mean}}$  represents the salinity flux ( $\overline{\mathbf{v}' S'}$ ) associated with the interannual anomalies across the mean salinity ( $\bar{S}$ ) surfaces. Following Hochet et al. (2020), this term is a source of variability when  $\overline{\mathbf{v}' S'}$  is directed opposite to the direction of the mean salinity gradient and a sink when it is directed in the same direction. The authors rationalized this term as a source when the interannual circulation acts to erode the mean salinity gradient (because the salinity flux is down-gradient) and as a sink when it acts to strengthen this mean gradient (the salinity flux is up-gradient). We will show below that in ECCO, the mean salinity in the BG increases with depth and outward from the center of the gyre. Therefore,  $\overline{\mathbf{v}' S'}$  is a source of variability when directed upward and/or toward the center of the BG. As shown in Appendix A, the opposite of this term appears in the square time-mean salinity budget and can, as a result, also be interpreted as a transfer of variance between the time-mean and interannual circulations.  $\text{VAR}_{\text{adv}}^{\text{eddy}}$  is the effect of the GM parameterized eddy induced velocities on the interannual salinity variance. In the same way as for  $\text{VAR}_{\text{adv}}^{\text{mean}}$ ,  $\text{VAR}_{\text{adv}}^{\text{eddy}}$  can be interpreted as a salinity flux ( $\overline{\mathbf{v}'_{\text{GM}} S'}$ ), albeit associated with eddy-induced parametrized velocities, across the mean salinity surfaces ( $\bar{S} = \text{constant}$  surfaces). As for  $\text{VAR}_{\text{adv}}^{\text{mean}}$ , it can also be interpreted as a transfer of variance between the time-mean and interannual circulations (see Appendix A). Lastly,  $\text{VAR}_{\text{adv}}^{\text{sub}}$  represents the effect of all sub-annual frequencies.

### 3. Model: The ECCO v4r3 State Estimate

We assess the salinity variance budget using the ECCO v4r3 state estimate. This state estimate is the output of the Massachusetts Institute of Technology general circulation model (MITgcm) assimilating available observations (Forget et al., 2015; Fukumori et al., 2017). The analysis presented in this article covers the period 1993–2014 where all the terms needed to close the tracer's budget are available. The advantage of ECCO over others reanalysis is that it satisfies the equation of motion and conservation laws hence making it possible to compute physically-sound tracers budget. The solution used in this article is computed on the LLC90 grid which has a horizontal resolution ranging from 111 km in the tropics to 40 km at high latitudes and 50 vertical levels with thickness ranging from 10 m at the surface to 450 m at depth. Mesoscale turbulence is therefore not resolved and its effect is parameterized using the Gent & McWilliams (GM) scheme (Gent & McWilliams, 1990). Unlike many other ocean model simulations that need to prevent drift due to errors in the surface freshwater flux forcing, ECCO v4, thanks to its assimilation procedure, does not relax sea surface salinity to a gridded observational product. 6-hourly ERA-Interim Reanalysis near-surface atmospheric state (wind stress, temperature, humidity downward radiation, precipitation) is used to force ECCO v4 (Forget et al., 2015). A seasonal climatology of runoff from Fekete et al. (2002) is added as part of the freshwater flux (Forget et al., 2015), implying that river discharge does not have interannual variations. The sea ice model is made of separate dynamic and thermodynamic elements that are coupled to the ocean model (Losch et al., 2010). In situ salinity observations used to constrain the state estimate in the Arctic are salinity profiles from Argo floats and the World Ocean Database (Antonov et al., 2010), salinity measurements from Ice Tethered Profilers (Toole et al., 2011) and mooring observations in the BG, Bering, Davis and Fram straits (Fukumori et al., 2017). We evaluate the ECCO v4 solution by comparing it to observations of freshwater content and sea ice thickness (Figure 1). Freshwater content is obtained by vertically integrating  $\frac{S_{\text{ref}} - S}{S_{\text{ref}}}$  between the surface and the  $S_{\text{ref}}$  isohaline with  $S_{\text{ref}} = 34.8$  psu following the canonical value used by Aagaard and Carmack (1989). Freshwater observations are obtained from the PHC 3.0 climatology (Steele et al., 2001) and sea ice thickness from the ESA Sea ice Climate Change Initiative (CCI) product

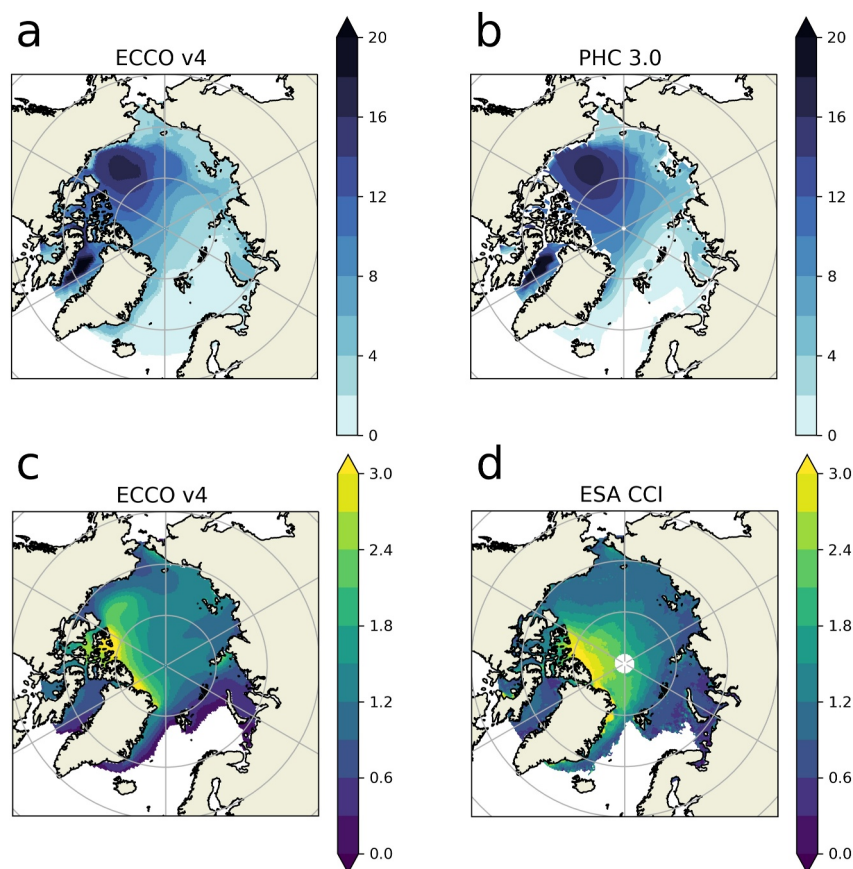


**Figure 1.** Comparison between ECCO v4 and observations. Time mean freshwater content ( $m$ ) for the period 1993–2014 in ECCO v4 (a) and in the PHC 3.0 climatology (b). Time mean sea-ice thickness ( $m$ ) for the Northern Hemisphere winter months (October through April) 2002–2014, in ECCO v4 (c) and in the ESA CCI product (d).

(Hendricks et al., 2018). ESA's CCI sea ice product is derived from satellite radar altimetry observations from Envisat (October 2002–October 2010) and CryoSat-2 (November 2010–April 2014). Note that the product is currently limited to the winter months of October through April due to unresolved bias in the remaining 5 months. Freshwater content in ECCO v4 (Figures 1a and 1b) is generally in good agreement with observations with the largest values (about 20 m) located in the BG. However, small differences can be found to the north of the BG, where the amount of freshwater is greater in observations than in ECCO v4. Sea ice thickness is in reasonable agreement with observations (Figures 1c and 1d), with the largest values (about 3 m) found along the north coast of Greenland and north of the Canadian Arctic Archipelago, and decreasing values toward the Siberian continent. However important differences are found around the North pole where observations give sea ice thickness values about  $\sim 1$  m larger than the ECCO v4 state estimate. Further assessment of the state estimate for the Arctic salinity can be found in Fournier et al. (2020).

#### 4. Results

Interannual anomalies are computed by subtracting the time mean seasonal cycle from the detrended monthly time series, then the sub-annual signal is removed using a Lanczos low-pass filter with a 1 year cutoff frequency. The interannual variability defined here thus contains all periods longer than 13 months. Note that we have checked that similar results holds with or without the long term (1993–2014) trend. The vertically integrated interannual variance in the Arctic region is the largest in the BG and along the Eastern Siberian Shelf (ESS) (Figure 2) with values above  $15 \text{ psu}^2 \text{ m}$ . These two regions have very different depths: the large variance from the BG is located in the Canadian Basin, which is as deep as 4500 m. On the contrary, the ESS is shallow (less than 100 m). In the remainder of this article, we use these two regions as well as the whole Arctic region to discuss our results. The BG region is defined using the standard BG box (e.g., Proshutinsky et al., 2009) characterized by

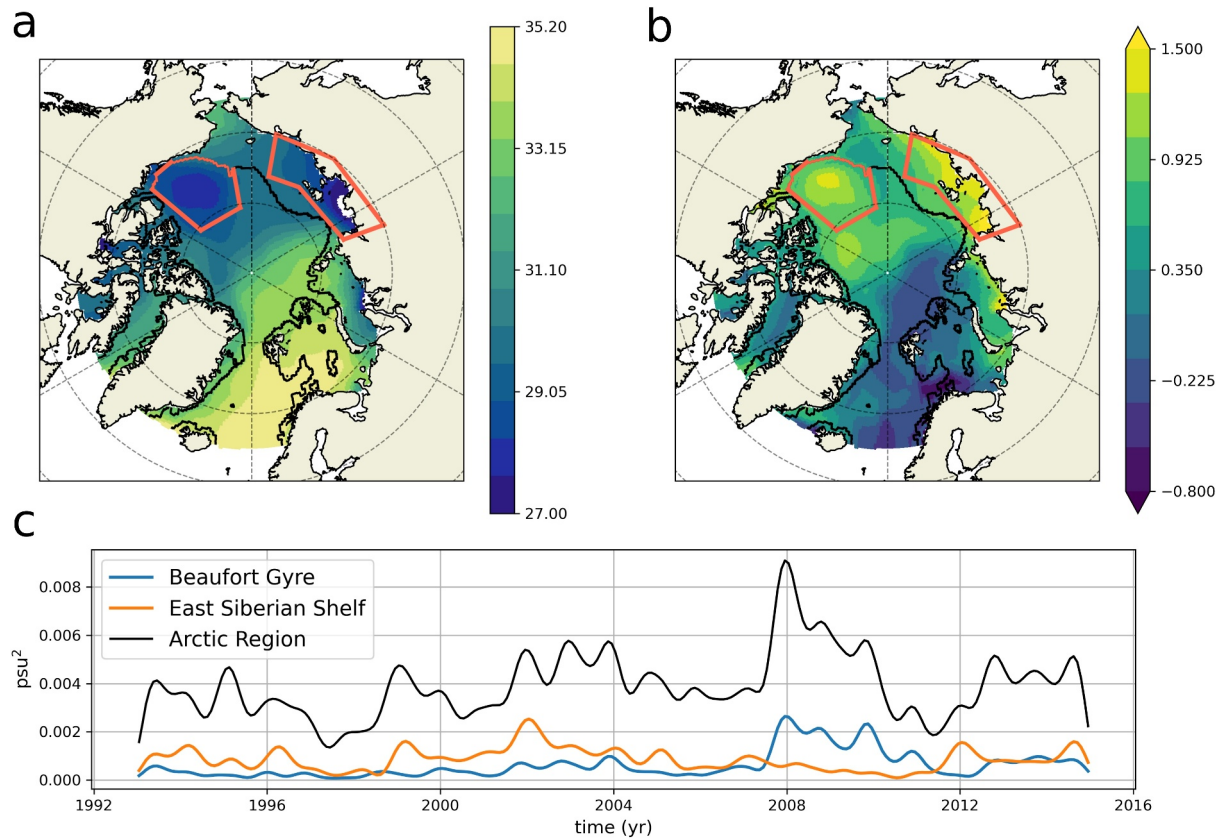


**Figure 2.** (a) Time mean surface salinity in the Arctic Basin (in psu) defined by latitudes North of 65°N. (b) log 10 of the vertically integrated variance of the interannual salinity anomaly (in psu<sup>2</sup> m) for the period 1993–2014. The two orange boxes show the location of the Beaufort Gyre (BG) and the East Siberian Shelf (ESS) boxes and the black contour shows the 300 m isobath. Panel (c): volume integral of the squared interannual salinity anomaly in the BG (blue line), ESS (orange line) and Arctic regions over the period 1993–2014. The three volume integrals are divided by the total Arctic volume.

latitudes between 70.5°N and 80.5°N and longitudes between 130°W and 170°W as well as by depths deeper than 300 m and shown by an orange box in Figure 2. We define the ESS region by latitudes between 70°N and 76°N and longitudes between 110°E and 170°E. The Arctic region is defined by all latitudes North of 65°N. The time series of the volume integrated squared salinity anomaly for each region is shown in Figure 2c. Each volume integral is divided by the Arctic volume, so that the contribution of the BG and ESS to the total Arctic region can be compared. Although the volume of the ESS region is small compared to the BG, the volume integral of the squared salinity is larger there than in the BG until 2007. This indicates that the interannual salinity variations are very intense in the ESS. After 2007 a large increase in squared salinity anomaly occurs in the BG which becomes larger than the ESS values. We will investigate the reasons for this increase in Section 5.

#### 4.1. Interannual Salinity Variance Budget

The vertical integral of the interannual salinity variance budget (Figure 3) shows the position and relative importance of the different terms in Equation 3. The surface freshwater forcing term  $VAR_{f_{fw}}$  (Figure 3b) is positive almost everywhere indicating that this term is a source of salinity variance. River runoffs do not contribute to  $VAR_{f_{fw}}$  because they are prescribed from a seasonal climatology in ECCO v4r3 (Forget et al., 2015). We have checked that  $VAR_{f_{fw}}$  is in fact mostly associated to interannual variations in sea ice melt and freezing. Its largest values are found in the East Siberian Shelf (ESS) where large salinity variance values are also found (Figure 2). It therefore suggests that the salinity variability in the ESS is mostly driven by interannual variations in the freshwater fluxes. Weaker positive values around 4 psu<sup>2</sup>yr<sup>-1</sup> m are found in the BG. The advective term exhibits regions with positive or negative values (Figure 3c), which means that this term can locally be a source or a sink of variability, depending on its location. Negative values of about 6 psu<sup>2</sup>yr<sup>-1</sup> m are found in the eastern part of the ESS region. In the BG region, positive values (~4 psu<sup>2</sup>yr<sup>-1</sup> m) are found on the outer part of the gyre and

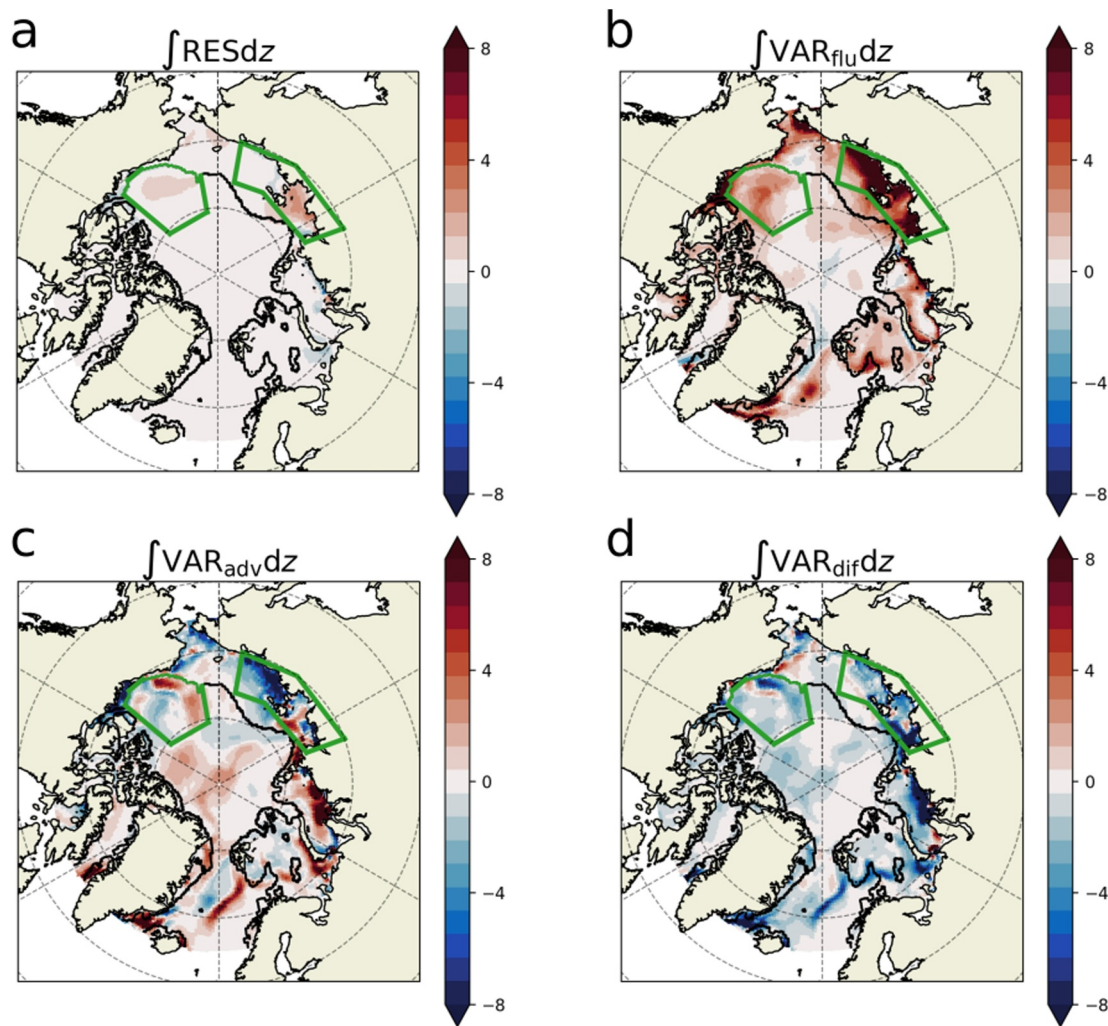


**Figure 3.** Vertical integral of the interannual salinity variance budget (in  $\text{psu}^2\text{yr}^{-1}\text{m}$ ). (a) Residual term—time-mean of the variance tendency, (b) surface freshwater fluxes variations, (c) advective terms, (d) diffusive terms. The two green boxes show the location of the Beaufort Gyre and East Siberian Shelf regions and the black contour shows the 300 m isobath.

weak negative values in its central part. The diffusive term is negative almost everywhere and is therefore almost exclusively a sink of variability (Figure 3d). The residual term related to the time mean of the salinity variance is, as expected for a long enough period, much weaker than the other three terms, indicating that we are close to a statistical equilibrium for the period considered (Figure 3a). It will thus be ignored in the remaining of the study. We further compute the volume integral of each of the four terms of the salinity variance budget (four first lines of Table 1) over the full volume encompassed in the Arctic Basin as well as over the BG and ESS regions (green boxes in Figure 3). Averaged over the Arctic basin, the main equilibrium is between the diffusive term (a sink) and the surface freshwater fluxes (a source). The volume average of the advective terms is negligible. Similar results hold for the BG, while in the ESS region the diffusive and advective terms both act as important sinks. We will show in a following section that the advective term can be decomposed into several terms that can be large but tend to closely compensate in the BG and over the Arctic basin.

#### 4.2. Insights Into the Advective Term

Following Equation 5, we decompose the advective term into several components. The vertical integral of each term of this decomposition (Figures 4a–4d) reveals that the main equilibrium is between (a) the term associated to the salinity flux across mean salinity surfaces (i.e.,  $\text{VAR}_{\text{adv}}^{\text{mean}}$ ) which is a source of variance and (b) the effect of the parameterized eddies (i.e.,  $\text{VAR}_{\text{adv}}^{\text{eddy}}$ ) which is a sink of variance.  $\text{VAR}_{\text{adv}}^{\text{eddy}}$  results from a strong compensation

**Table 1**

*Volume Integral of the Interannual Salinity Variance Budget Terms for the Arctic Region (second Column), Beaufort Gyre (Third Column) and East Siberian Shelf Region (Last Column)*

	Arctic region	Beaufort gyre	East Siberian shelf
RES	0.6	0.9	2.3
VAR <sub>dif</sub>	-115.2 (24%)	-8.7 (10%)	-15.0 (27%)
VAR <sub>flu</sub>	116.9 (25%)	9.1 (10%)	35.4 (61%)
VAR <sub>adv</sub>	-1.1	0.5	-18.1
VAR <sub>adv</sub> <sup>mean</sup>	302.1 (63%)	77.4 (84%)	22.5 (39%)
VAR <sub>adv</sub> <sup>adv</sup>	57.6 (12%)	5.3 (6%)	-3.9 (7%)
VAR <sub>adv</sub> <sup>eddy</sup>	-307.9 (65%)	-78.5 (86%)	-25.4 (46%)
VAR <sub>adv</sub> <sup>sub</sup>	-52.9 (11%)	-3.7 (4%)	-11.3 (20%)

*Note.* To be consistent with Figure 2, values for the three regions are scaled by the inverse of the total Arctic volume and units is  $10^{-5} \text{ psu}^2 \text{ yr}^{-1}$ . In each column, blue (red) percentage represents the relative contribution of each term for the total sink (source) of the corresponding region. Note that the sum of  $\text{VAR}_{\text{adv}}^{\text{mean}}$ ,  $\text{VAR}_{\text{adv}}^{\text{adv}}$  and  $\text{VAR}_{\text{adv}}^{\text{eddy}}$  is equal to  $\text{VAR}_{\text{adv}}$ . The physical interpretation for each term is given in Figure 5.

between its horizontal and vertical parts (not shown). These two terms have large amplitudes in the BG, around  $\pm 16 \text{ psu}^2 \text{ yr}^{-1} \text{ m}$ , where the variance is also found to be maximum (Figure 2). The two terms are also in close balance as apparent from the sum of all advective terms (i.e.,  $\text{VAR}_{\text{adv}}$ , Figure 3c) which does not present any local maximum or minimum in the BG, contrary to  $\text{VAR}_{\text{adv}}^{\text{eddy}}$  and  $\text{VAR}_{\text{adv}}^{\text{mean}}$ . This main balance is in agreement with previous results on the main mechanisms of freshwater content variability in the BG based on theoretical arguments or idealized process models (e.g., Manucharyan et al., 2016) (see also Section 4.4). Here we show that this balance also holds in a realistic configuration, that captures more processes and an increased level of complexity. The same balance also holds in most of the deep regions of the Arctic (delimited by the 300 m isobath in Figure 4), albeit with smaller amplitudes. Large positive values of  $\text{VAR}_{\text{adv}}^{\text{mean}}$  ( $\pm 16 \text{ psu}^2 \text{ yr}^{-1} \text{ m}$ ) are also found in the Chukchi Sea, compensated by large negative values of  $\text{VAR}_{\text{adv}}^{\text{eddy}}$  (Figures 4a and 4b), indicating a similar balance in this region. In the ESS,  $\text{VAR}_{\text{adv}}^{\text{mean}}$  is positive and has high values in the western part.  $\text{VAR}_{\text{adv}}^{\text{eddy}}$  can be positive in some localized regions of the ESS, but as the volume integral calculation shows (see below), it is actually mostly negative in this region and thus a sink for salinity variance.

The term associated with the advection of salinity variance  $\text{VAR}_{\text{adv}}^{\text{adv}} = \overline{S' \text{adv}'_{\text{adv}}}$  is mostly positive and can be locally important over the ESS (Figure 4c), with values up to  $16 \text{ psu}^2 \text{ yr}^{-1} \text{ m}$ . Interestingly, it is weakly negative in the center of the BG (i.e., a sink of variability), and positive on the southern boundaries of the gyre (i.e., a variability source), suggesting a southward transport of variability from the center of the gyre. Table 1 shows the volume average of the different advective terms over the Arctic basin for the 1993–2014 period (second column). There are three sources of variance: the main source ( $\text{VAR}_{\text{adv}}^{\text{mean}}$ ) is linked to a transfer of variance between the mean and interannual circulations and represents 63% of all sources, the second one is associated to freshwater fluxes variations ( $\text{VAR}_{\text{flu}}$ , 25%), the third is the advection of variance from sub-Arctic regions ( $\text{VAR}_{\text{adv}}^{\text{adv}}$ , 12%). Indeed, the volume integral of  $\text{VAR}_{\text{adv}}^{\text{adv}}$  can be written as:

$$\int_{\mathcal{V}} \text{VAR}_{\text{adv}}^{\text{adv}} \text{d}\mathcal{V} = - \int_{\sigma} V_n \frac{(S')^2}{2} \text{d}\sigma, \quad (7)$$

where  $\mathcal{V}$  is a volume (and  $\text{d}\mathcal{V}$  is the volume unit),  $\sigma$  represents its surface boundary (and  $\text{d}\sigma$  is the volume surface), and  $V_n = \mathbf{V} \cdot \mathbf{n}$  is the velocity across the surface of the volume (where  $\mathbf{n}$  is the unit vector normal to this surface and directed toward others regions). This equation shows that the volume integral of the term linked with the variance advection is equal to the flux of salinity variance through its boundaries ( $\sigma$ ), which represents the divergence of the salinity variance flux. Thus, if the volume integral of  $\text{VAR}_{\text{adv}}^{\text{adv}}$  is positive, then the interannual variability of salinity is imported from other regions whereas it is exported when the term is negative. Inflows or outflows from subarctic regions therefore contribute to  $\text{VAR}_{\text{adv}}^{\text{adv}}$ . As the term linked with the advection of variance is a relatively small source of Arctic salinity variance, it implies that (a) 88% of the Arctic salinity variance is generated locally in the Arctic and (b) overall, in ECCO and over the 1993–2014 period, the Arctic region imports salinity variance from the sub-Arctic regions rather than exporting it. Yet, one needs to remember that the Arctic is connected with the subarctic regions through different sections: the Bering strait connecting the Arctic to the North Pacific and the Canadian Archipelago, Fram Strait and the Barents Sea Opening connecting the Arctic to the North Atlantic. Thus it cannot be ruled out that a strong compensation occurs between these different sections and that larger amounts of variance are imported and exported through individual sections. It was found for instance that the variations of freshwater transport along both sides of Greenland can be strongly anti-correlated in some global models (Wang et al., 2016). However, exploring this question is beyond the scope of this article. The vertical integral of the term representing the effect of all sub-annual frequencies (i.e.,  $\text{VAR}_{\text{adv}}^{\text{sub}}$ ) is a weak sink of salinity variability and has amplitudes much weaker than the three other terms (Figure 4d).



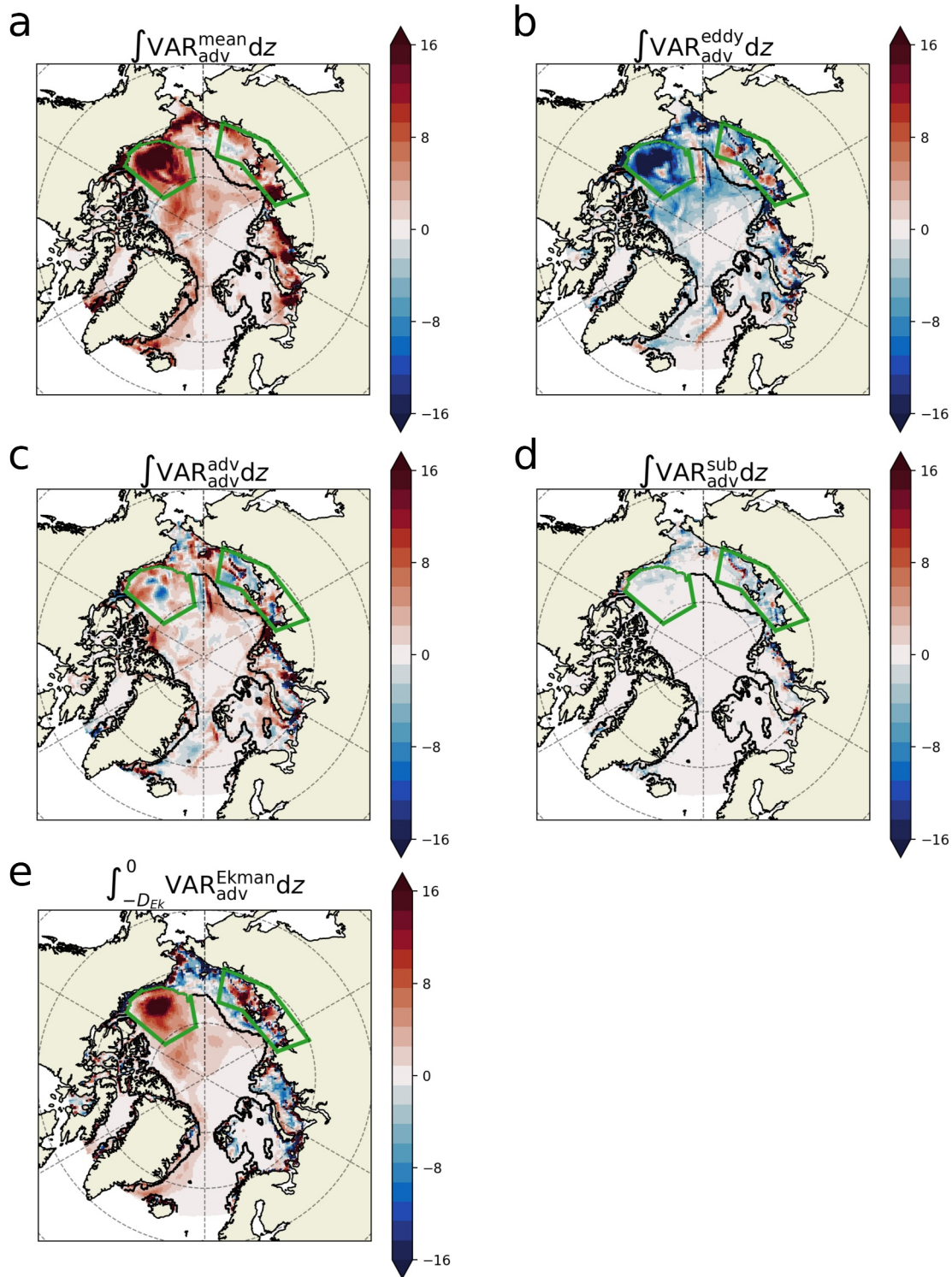


**Figure 4.** Vertical integral of the decomposition of the advective term into four components (in  $\text{psu}^2\text{yr}^{-1}\text{m}$ ) as described by Equation 6. (a) Term linked to the resolved salinity flux across mean salinity surfaces, (b) effect of the GM parametrization of eddies, (c) advection of interannual salinity variance by resolved and eddy induced mean and interannual velocities and panel (d) effect of sub-annual frequencies. (e) vertical integral of the reconstruction of the term  $\text{VAR}_{adv}^{\text{mean}} = \overline{S' \text{adv}'_{\text{mean}}}$  using Ekman velocities (see Section 4.3). The two green boxes show the location of the Beaufort Gyre and East Siberian Shelf regions and the black contour shows the 300 m isobath.

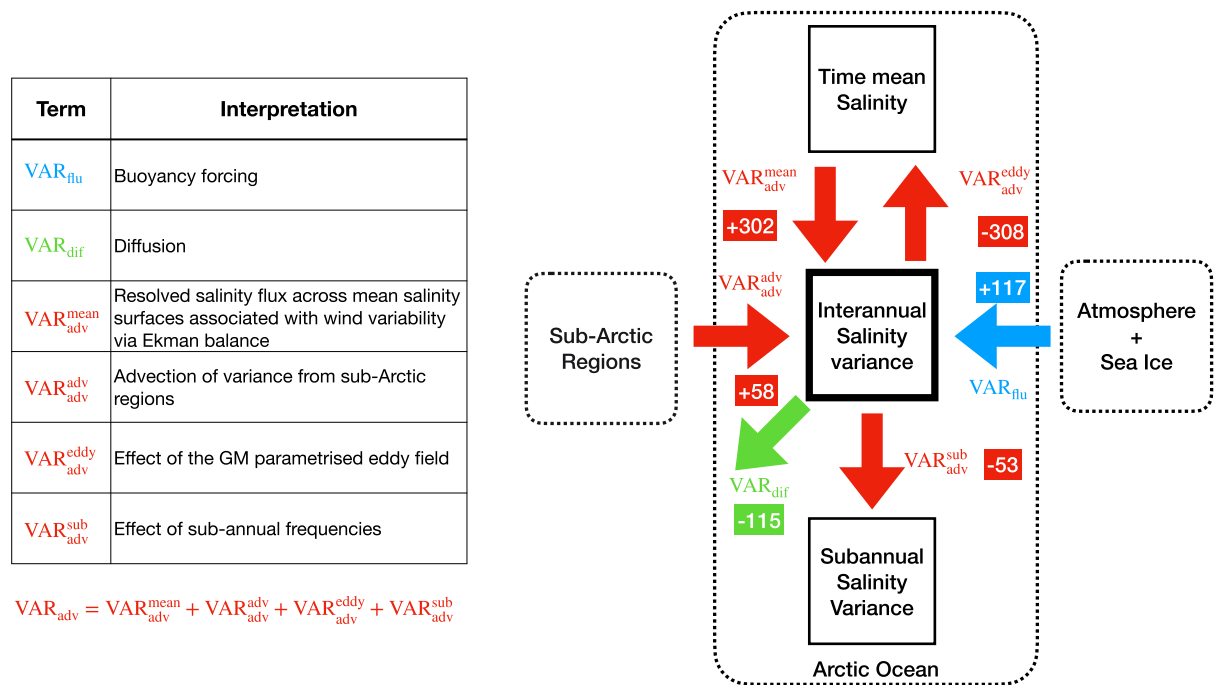


**Figure 5.** Schematic view of the salinity variance budget integrated over the Arctic volume. The thick square represents the interannual salinity variance reservoir considered in this article while the two other squares represent the mean circulation (top) and the sub-annual salinity anomalies variance reservoir (bottom). These three reservoirs are located within the Arctic volume shown by a dashed black box. Each of the six arrows represents one of the six terms of the salinity variance budget for the Arctic region shown in Table 1. Values corresponding to the Arctic region volume integral of each salinity variance budget term, scaled by the Arctic volume, are also given (unit:  $10^{-5}$   $\text{psu}^2\text{yr}^{-1}$ , see also Table 1). The four advective transfer terms are shown in red, the diffusive transfer is in green and the buoyancy forcing transfer term is in blue. If the arrow is directed toward the interannual salinity variance then it is a source of salinity variance while it is a sink otherwise. The sub-Arctic regions and atmosphere plus sea ice compartment are represented by two dashed black boxes to outline respectively the advection of variance from sub-Arctic regions and the buoyancy forcing from Atmosphere (evaporation precipitation and river runoff) and sea ice melt and freezing. The different terms of the budget and their respective interpretation are shown in the left table. Note that  $VAR_{adv}^{mean}$  and  $VAR_{adv}^{eddy}$  act as transfers of salinity variance between the mean and interannual circulations in opposite directions.

Table 1 also provides the volume integral of the budget separately for the BG, ESS, and Arctic regions over the 1993–2014 period. The importance of each term in contributing to the total source (in red) or sink (in blue) is given as a percentage. The volume integral in the BG confirms that the salinity variability in this region is mostly forced (84% of all sources) by the advective term linked with resolved salinity flux across mean salinity surfaces  $VAR_{adv}^{mean}$ . The main sink (86%) is associated with the parametrized eddy turbulence ( $VAR_{adv}^{eddy}$ ). In the ESS, the dynamics appear to be fundamentally different. In this region, the main source is indeed associated to the buoyancy forcing ( $VAR_{flu}$ , 61%) and secondarily to  $VAR_{adv}^{mean}$  (39%). The main sink is associated to the parametrized eddy turbulence (46%), and to the diffusion (27%).

To summarize this section, a schematic view of the variance budget for the Arctic basin is given in Figure 5 as well as the physical interpretation for each terms of the budget.

### 4.3. Role of the Wind in Sustaining the Salinity Variability

In most of the previous studies performing buoyancy or temperature variance budgets (e.g., Arzel et al., 2018; Colin de Verdière & Huck, 1999; Hochet et al., 2015; Hochet et al., 2020), the term associated to the buoyancy flux across the mean buoyancy surfaces ( $VAR_{adv}^{mean}$  here) is described as the signature of a baroclinic instability. Recently, Hochet et al. (2023) have shown in the context of steric sea level variability that it can also be the signature of wind variability via Ekman balance. In this section, we employ a similar methodology as in Hochet et al. (2023) to assess if the main source of interannual salinity variance (i.e., the term  $VAR_{adv}^{mean}$ , Figures 4a and Table 1) can be attributed to wind variations. To do so, we reconstruct a term similar to  $VAR_{adv}^{mean}$ , that we call  $VAR_{adv}^{EKman}$ , except that the velocity field is replaced by the interannually-varying Ekman velocities in the Ekman layer. The methodology to obtain these velocities is described hereafter. We assume that the horizontal Ekman

velocities are zero below the Ekman layer (i.e.,  $z < D_{\text{Ek}}$ ), depth independent in the Ekman layer (for  $0 \geq z \geq D_{\text{Ek}}$ ) and given by:

$$(u_{\text{Ek}}, v_{\text{Ek}}) = \frac{1}{D_{\text{Ek}} f_0 \rho_0} (\tau_y^{\text{Ocean}}, -\tau_x^{\text{Ocean}}) \quad (8)$$

where  $f_0$  is the Coriolis parameter,  $\rho_0$  is the reference density, and  $(\tau_x^{\text{Ocean}}, \tau_y^{\text{Ocean}})$  are the zonal and meridional components of the interannual momentum stress anomaly received by the ocean at its surface (i.e., from the ice or the atmosphere depending if the ocean is sea-ice covered or not at the studied location, respectively). The vertical Ekman velocity in the Ekman layer is then obtained from the vertical integral of the continuity equation as:

$$w_{\text{Ek}}(z) = -z \left( \frac{\partial u_{\text{Ek}}}{\partial x} + \frac{\partial v_{\text{Ek}}}{\partial y} \right) \quad (9)$$

We then use the 3D Ekman velocity  $\mathbf{v}'_{\text{Ek}} = (u_{\text{Ek}}, v_{\text{Ek}}, w_{\text{Ek}})$  to construct  $\text{VAR}_{\text{adv}}^{\text{Ekman}}$  as follows:

$$\text{VAR}_{\text{adv}}^{\text{Ekman}} = \overline{S' \text{adv}'_{\text{Ekman}}} = -\overline{S' \mathbf{v}'_{\text{Ek}} \cdot \nabla \bar{S}} \quad (10)$$

$\text{VAR}_{\text{adv}}^{\text{Ekman}}$  is then vertically integrated over the depth of the Ekman layer in order to compare it with the vertical integral of  $\text{VAR}_{\text{adv}}^{\text{mean}}$ :

$$\int_{D_{\text{Ek}}}^0 \text{VAR}_{\text{adv}}^{\text{Ekman}} dz \quad (11)$$

where the Ekman layer depth  $D_{\text{Ek}}$  is assumed everywhere constant. We choose to use  $D_{\text{Ek}} = 50$  m but we find that the reconstruction in the Ekman layer is almost insensitive to the choice of  $D_{\text{Ek}}$ . The vertical integral of  $\text{VAR}_{\text{adv}}^{\text{Ekman}}$  (i.e., Equation 11) in the Ekman layer is shown in Figure 4d. Strong positive values (around  $16 \text{ psu}^2 \text{ yr}^{-1} \text{ m}$ ) are found in the BG and weaker values along the eastern coast of Greenland and in the deep regions of the Arctic, with a pattern very similar to the vertical integral of  $\text{VAR}_{\text{adv}}^{\text{mean}}$  (Figure 4a). This suggests that a large part of the main source of variability is sustained by wind variations. However some important differences exist, particularly in shallow depth regions and on the ESS where Ekman velocities induce more negative values and more intense positive values than the ones of  $\text{VAR}_{\text{adv}}^{\text{mean}}$ . The large positive values of  $\text{VAR}_{\text{adv}}^{\text{mean}}$ , found in the Chukchi Sea (Figure 4), are also not present in the Ekman reconstruction. Therefore, other processes (such as large-scale baroclinic instability, Colin de Verdière & Huck, 1999; Hochet et al., 2015; Gastineau et al., 2018) might be at play in this region but we leave this subject to future investigations.

#### 4.4. Link With the Residual Mean Theory Applied to the Beaufort Gyre Freshwater Variability

As already mentioned in the introduction, several studies have investigated the dynamics at play controlling the freshwater variability in the BG based on a residual-mean framework (Manucharyan et al., 2016; Manucharyan & Spall, 2016; Timmermans & Marshall, 2020), which was originally developed to understand the dynamics of the Southern Ocean (Marshall & Radko, 2003). We show here how the different terms of the residual mean framework can be recovered from our salinity variance budget. In Manucharyan et al. (2016), the linearization of the equation controlling the salinity variations in the BG, away from any boundary, gives the following equation (see their Appendix A):

$$\frac{\partial S'}{\partial t} + \nabla \cdot (\mathbf{v}' \bar{S}) + \nabla \cdot (\mathbf{v}'_* \bar{S}) = 0 \quad (12)$$

where  $S'$  is the salinity anomaly,  $\mathbf{v}'$  is the anomalous velocity and is assumed to be entirely due to surface stress anomalies via Ekman dynamics in this framework, and  $\mathbf{v}'_*$  is the eddy induced or bolus velocity. Note that the advection of  $S'$  by the mean residual velocity is zero in Equation 12 because these two circulations exactly compensate in this framework. Manucharyan et al. then used this equation to derive an evolution equation of the

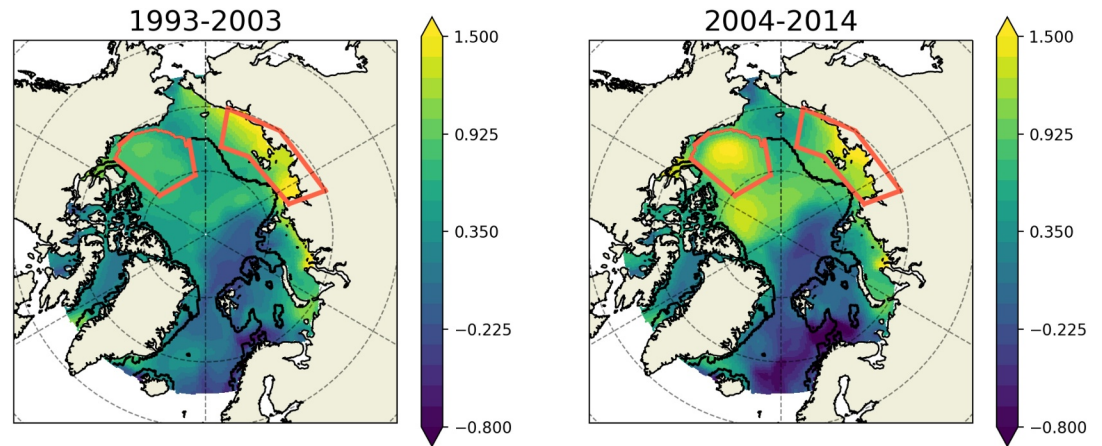


**Figure 6.** Vertical integral of the interannual salinity variance (i.e.  $\int S'^2 dz$  in  $\text{psu}^2 \text{m}$ ) computed with respect to the 1993–2014 mean for the periods 1993–2003 (left panel) and 2004–2014 (right panel). The two orange boxes show the location of the BG and ESS regions and the black contour shows the 300 m isobath.

halocline depth anomalies (see their Appendix A). Here, our approach is different: we seek the sources and sinks of the salinity variability. To see how this apply to Equation 12, we follow the same procedure as above by computing the time average of the product of  $S'$  and Equation 12, that is:

$$\overline{\mathbf{v}' S'} \cdot \nabla \bar{S} = -\overline{\mathbf{v}'_* S'} \cdot \nabla \bar{S} \quad (13)$$

where a statistical steady state has been assumed so that the term involving the time derivative disappears. This equation shows that the transport of anomalous salinity  $S'$  made by the wind across mean salinity surfaces must be exactly compensated by the eddy transport of  $S'$  across the same surfaces. The two terms in Equation 13 are also found in the decomposition of the advective terms of the salinity variance budget Equation 6. Indeed, the first term of this equation ( $\overline{\mathbf{v}' S'} \cdot \nabla \bar{S}$ ) corresponds to  $\text{VAR}_{\text{adv}}^{\text{mean}}$ , or even  $\text{VAR}_{\text{adv}}^{\text{Ekman}}$ , in Equation 6 (see also Appendix A). The second term ( $\overline{\mathbf{v}'_* S'} \cdot \nabla \bar{S}$ ) corresponds to  $\text{VAR}_{\text{adv}}^{\text{eddy}}$ . We have shown in the previous sections (and in Figure 4) that these terms are the two dominant terms of the salinity variance budget in the BG, in agreement with idealized model studies (Manucharyan et al., 2016). However, comparing Equation 13 with the combination of Equation 3 and 6 (Figures 3 and 4, respectively), reveals that several non-negligible terms are missing from Equation 13. In particular, the effect of the diffusive and freshwater fluxes is missing. These two terms are a sink and a source of variability and represent both 10% of the total sink and total source for the BG. Moreover, the comparison of the term  $\text{VAR}_{\text{adv}}^{\text{mean}}$  (Figure 4a) and its reconstruction from Ekman velocities  $\text{VAR}_{\text{adv}}^{\text{Ekman}}$  (Figure 4d) suggests that the wind variations do not account for all the sources. Therefore, our study suggests that a significant part of the anomalous velocity field is not the result of an Ekman balance contrary to what is generally assumed in idealized models of the BG.

## 5. Recent Changes of the Salinity Variance Budget

Large changes of the Arctic freshwater budget and content have been observed over the past two decades (e.g., Haine et al., 2015; Rabe et al., 2014; Timmermans & Toole, 2023). We thus investigate if these changes in salinity were potentially accompanied by changes of the salinity variance. To that aim, we compare the variance budget over two periods (1993–2003 and 2004–2014), and decompose the salinity variance into two terms as follows:

$$\overline{S'^2} = \frac{1}{2} \left( \overline{S'^2}^{93-03} + \overline{S'^2}^{04-14} \right), \quad (14)$$

where  $\overline{S'^2}^{93-03}$  and  $\overline{S'^2}^{04-14}$  are respectively the squared salinity anomaly (with respect to the 1993–2014 time mean) averaged over 1993–2003 and 2004–2014. This reveals large differences of the interannual salinity variance between the two periods (Figure 6 and Table 2), especially over the BG where the level variability is

**Table 2**

*Percentage of Increase or Decrease in the Amplitude of the Volume Average of Each Term From the Salinity Variance Budget for the Period 2004–2014 With Respect to 1993–2003*

	Beaufort gyre	East Siberian shelf
$S'^2$	+158%	−28.5%
$\text{VAR}_{\text{adv}}^{\text{mean}}$	+353%	−64%
$\text{VAR}_{\text{adv}}^{\text{eddy}}$	+260%	−38%
$\text{VAR}_{\text{dif}}$	+2 140%	−14%
$\text{VAR}_{\text{flu}}$	+91%	−15%
$\text{VAR}_{\text{adv}}^{\text{adv}}$	+109%	−73%
$\text{VAR}_{\text{adv}}^{\text{sub}}$	+234%	−9%

*Note.* Results are shown for the Beaufort gyre (second column) and East Siberian Shelf region (last column). In each column, a + (−) sign indicates that the amplitude has increased (decreased). In the first row, the corresponding percentage increase or decrease in volume averaged salinity variance is also given. The physical interpretation for each term is given in Figure 5. The amplitude of each term can be seen in Figures 8 and 9.

much larger in the second period than in 1993–2003, and over the ESS where the variance tends to reduce in the second period. The volume averaged salinity variance underwent a 158% increase in the BG and a 29% decrease in the ESS in the second period with respect to the first.

The increase in salinity variance of the BG is consistent with its intensification and expansion after 2007 documented by Armitage et al. (2017), Regan et al. (2019) using satellite-derived observations of geostrophic velocities. This intensification was due to a positive anomaly of the Beaufort High over the same period of time and to the reduction of the sea ice extent and thickness. Neglecting the time-independent terms in Equation 5, the time evolution of the squared salinity anomaly becomes:

$$\frac{1}{2} \frac{\partial S'^2}{\partial t} \approx S' \text{adv}'_{\text{mean}} + S' \text{adv}'_{\text{eddy}} + S' \text{adv}'_{\text{adv}} + S' \text{adv}'_{\text{sub}} + S' \text{flu}' + S' \text{dif}' \quad (15)$$

The time series of the volume integral of this equation over the 1993–2014 period is computed for the BG, ESS, and Arctic regions (Figure 7). A regime shift is apparent between the two periods for the three regions. In the BG, a large increase in amplitude occurs (Figure 7, top panel). It is linked to

the salinity flux across mean salinity surfaces ( $S' \text{adv}'_{\text{mean}}$ ) and correspondingly in the parameterized eddy turbulence term ( $S' \text{adv}'_{\text{eddy}}$ ). This increase is also visible for the full Arctic Basin, albeit with a smaller amplitude (Figure 7, bottom panel). The larger values obtained in the Arctic Basin for  $S' \text{adv}'_{\text{mean}}$  and  $S' \text{adv}'_{\text{eddy}}$  compared to the BG (about two times larger) suggest that regions outside the BG and ESS are also affected by the amplitude increase. In contrast, the ESS is characterized by a weaker variance in the second period compared to the first (Figure 7, middle panel), associated with a decrease of the variability of almost all terms from Equation 15. Hence it further highlights that the dynamics controlling the interannual variability in salinity differs between the BG and the ESS.

To better understand the spatial distribution of each term during the two periods, we compute the time average of the vertical integral of  $S' \text{adv}'_{\text{mean}}$  and  $S' \text{adv}'_{\text{eddy}}$  over 1993–2003 and 2004–2014. Consistently with their spatial averages,  $\text{VAR}_{\text{adv}}^{\text{mean}} = \overline{S' \text{adv}'_{\text{mean}}}$  in the BG is larger during 2004–2014 period than during the 1993–2003 period (Figure 8b vs. Figure 8a), and hence a larger source of variability. Similarly,  $\text{VAR}_{\text{adv}}^{\text{eddy}} = \overline{S' \text{adv}'_{\text{eddy}}}$  is more negative in the BG for the second period which indicates that it is a stronger sink of variability (Figure 8c vs. Figure 8d). Over the ESS,  $\text{VAR}_{\text{adv}}^{\text{mean}}$  and  $\text{VAR}_{\text{adv}}^{\text{eddy}}$  both have larger amplitudes in the first period (in agreement with Figure 7). In the deep Arctic basins,  $\text{VAR}_{\text{adv}}^{\text{mean}}$  and  $\text{VAR}_{\text{adv}}^{\text{eddy}}$  also have larger amplitudes in the second period. In the Chukchi Sea, large positive values of  $\text{VAR}_{\text{adv}}^{\text{mean}}$  are found near the Siberian side in the first period and shift to the Alaskan side in the second period. The amplitude of the term  $\text{VAR}_{\text{adv}}^{\text{eddy}}$  follows the same path. To quantitatively estimate the changes we have computed the percentage of increase or decrease in the period 2004–2014 with respect to 1993–2003 for each term of the variance budget integrated over the volume of the BG and ESS regions (Table 2). In the BG the volume integral of  $\text{VAR}_{\text{adv}}^{\text{mean}}$  and  $\text{VAR}_{\text{adv}}^{\text{eddy}}$  increases respectively by 353% and 260% in the second period while in the ESS it decreases by 64% and 38%.

We further average the reconstruction of  $S' \text{adv}'_{\text{mean}}$  from Ekman velocities ( $S' \text{adv}'_{\text{Ekman}}$ ), following the method described in Section 4.3, over the two periods (Figures 8e and 8f). The reconstruction follows the vertical integral of  $\overline{S' \text{adv}'_{\text{mean}}}$  averaged over the same periods (Figures 8a and 8b). Indeed, the time average over the second period (Figure 8f) is much larger (around 32  $\text{psu}^2\text{yr}^{-1}\text{m}$ ) in the BG than over the first period (around 10  $\text{psu}^2\text{yr}^{-1}\text{m}$ ); (Figure 8e). It suggests that, in the BG, it is the intensification of wind variability in the second period that leads to a larger source of variability and thus to larger salinity variability over the second period. We have verified that it is indeed the wind change and not changes of the sea ice conditions in the second period that leads to this larger source of variability. As a response,  $\overline{S' \text{adv}'_{\text{eddy}}}$  amplitude also increases to compensate this wind-driven variance

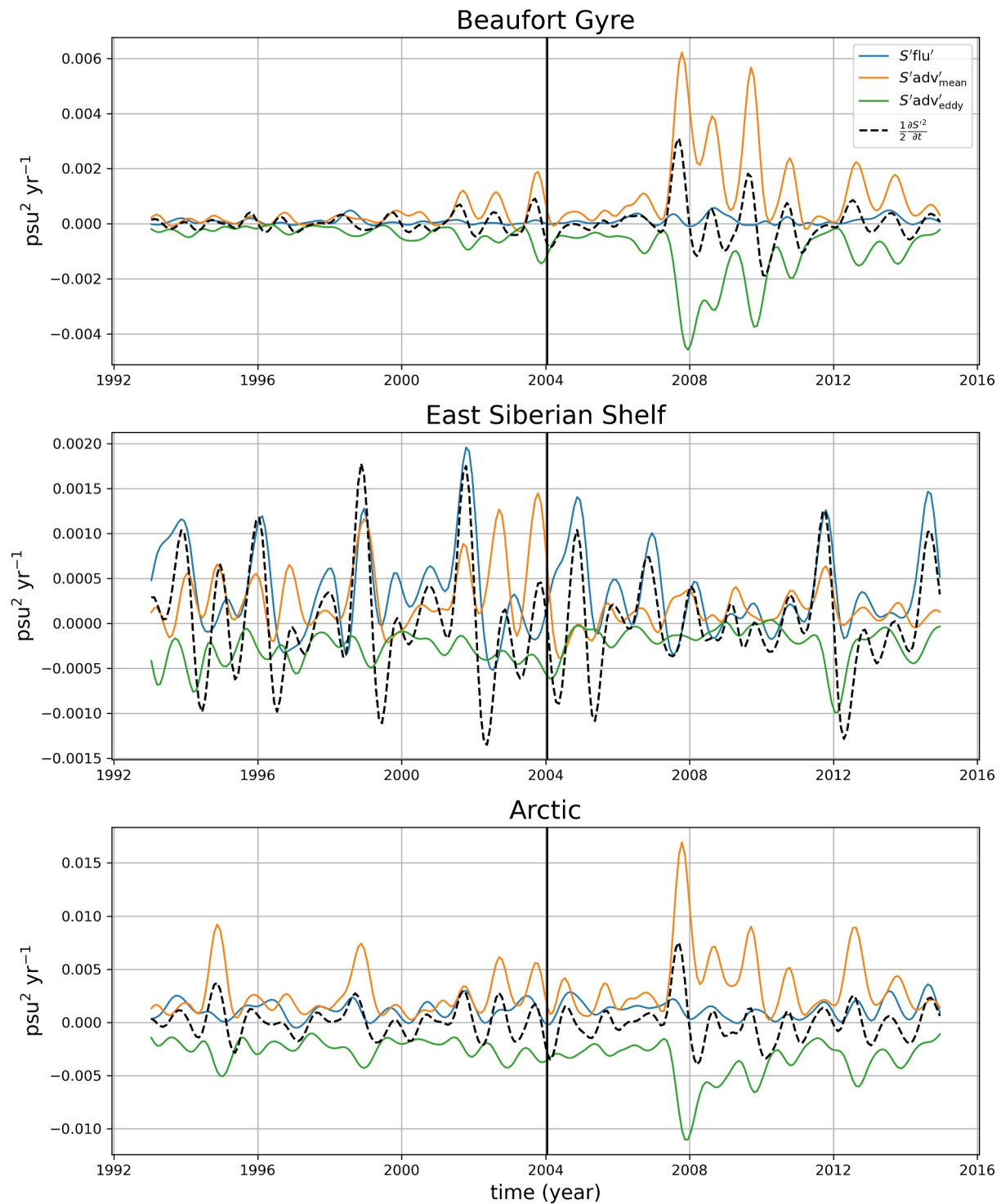


**Figure 7.** Time series of the volume integral of salinity variance budget terms for the BG (top panel), East Siberian Shelf (middle panel) and Arctic region (bottom panel). Each region is scaled by the inverse of the Arctic volume and units is  $\text{psu}^2\text{yr}^{-1}$ . For the sake of clarity we only show the dominant terms. Buoyancy forcing is shown in blue, the effect of parameterized eddies in green, the term linked with the salinity flux across mean salinity surfaces in orange and the time variations of the variance in dash black. The vertical black line represents the separation between the two periods (1993–2003 and 2004–2014) as described in the text.

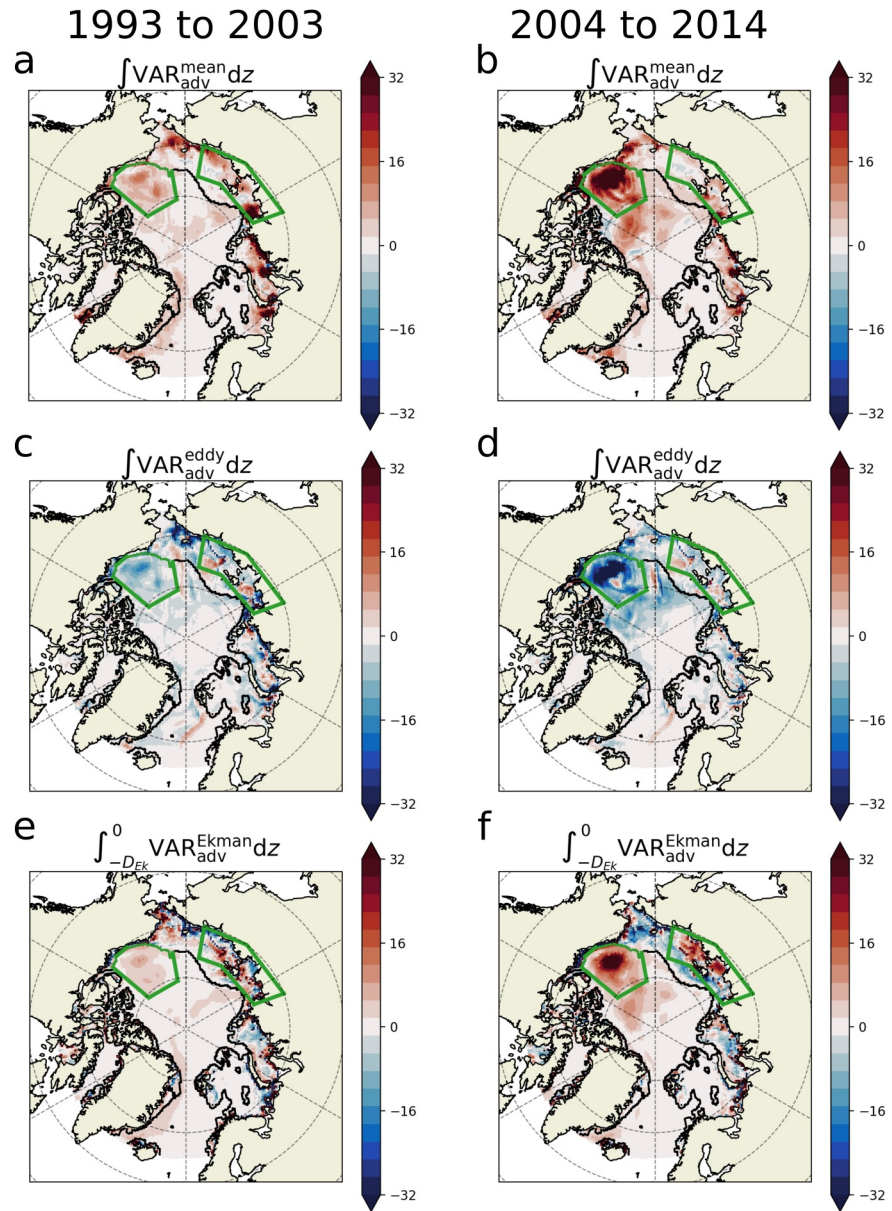


**Figure 8.** (a, b) Vertical integral of the salinity flux across mean salinity surfaces (in  $\text{psu}^2\text{yr}^{-1}\text{m}$ ). (c, d) Effect of the GM parameterization of eddies. (e, f) Vertical integral of the reconstruction of the term  $\overline{S'adv'_{\text{mean}}}$  using Ekman velocities ( $S'adv'_{\text{Ekman}}$ ). The left column shows the time average over the period 1993–2003 (a, c, and e) and the right column the time average over the period 2004–2014 (b, d, and f). The green boxes show the BG and ESS regions and the black contour shows the 300 m isobath.

source. The equation for  $\text{VAR}_{\text{adv}}^{\text{eddy}}$  ( $\text{VAR}_{\text{adv}}^{\text{eddy}} = -\overline{v'_{\text{GM}}S' \cdot \nabla \overline{S}}$ ) suggests that this increase is due to both the increase in salinity anomalies and the increase of GM velocities associated to steeper isopycnal slopes.

The time average of the vertical integral of  $\text{VAR}_{\text{flu}} = \overline{S' \text{flu}'}$  for the two periods (Figures 9a and 9b) shows that this source term increases in the BG (+91%, see Table 2) and decreases in the ESS (−15%). In the ESS, large localized values of the vertical integral of  $\text{VAR}_{\text{flu}}$  are found close to the coast in the first period while the second period is characterized by more uniform values. In the Chukchi Sea,  $\text{VAR}_{\text{flu}}$  is an important source of variance in the first period and it is mostly localized on the Siberian side of the Bering Strait. It becomes much less intense in the second period. In the BG, the vertical integral of the term associated with the advection of the salinity variance

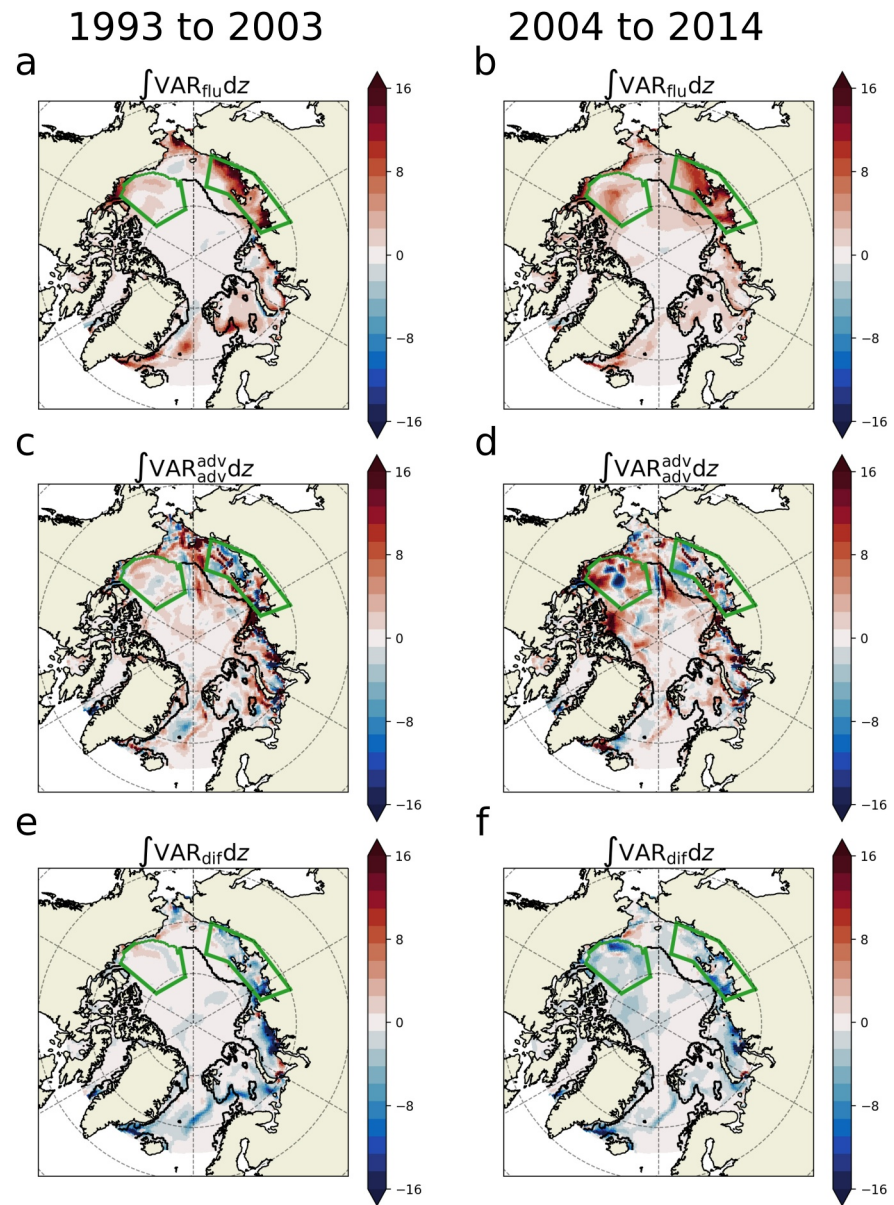


**Figure 9.** Same as Figure 8 but for the vertical integral of the term linked with the freshwater fluxes (panels a and b, in  $\text{psu}^2\text{yr}^{-1}\text{m}$ ), the vertical integral of the term linked with the advection of salinity variance (panels c and d) and the term linked with the diffusion (panels e and f).

$(\text{VAR}_{\text{adv}}^{\text{adv}} = \overline{S' \text{adv}'_{\text{adv}}})$  (Figures 9c and 9d) is intensified in the second period with negative values in the gyre center (thus a sink of salinity variance) and positive values along its boundary (thus a source of salinity variance). An increase in the amplitude of this term is also found in most of the deep Arctic. In the ESS,  $\text{VAR}_{\text{adv}}^{\text{adv}}$  can be a source or a sink depending on the location and its amplitude decreases over the second period. Overall, the volume integral of  $\text{VAR}_{\text{adv}}^{\text{adv}}$  increases by 109% in the BG and decreases by 73% in the ESS in the second period (Table 2). A strong increase (+2 140%, Table 2) in the amplitude of the vertical integral of the diffusive term  $(\text{VAR}_{\text{dif}} = \overline{S' \text{dif}'})$  occurs in the second period in the BG. This is explained by the fact that, in the first period, weak negative values of the vertical integral of  $\text{VAR}_{\text{dif}}$  are found in some parts of the BG and are compensated by weak positive values in other parts which thus result in a weak overall value of the volume integral of  $\text{VAR}_{\text{dif}}$ . On the contrary, in the second period, the increase in wind forcing found over the BG leads to strong negative values



of  $VAR_{dif}$ , particularly in the south-western part of the gyre (Figures 9e and 9f) and thus explains the very large relative increase of the volume integral of  $VAR_{dif}$ . Since there is a strong link between vertical diffusion and the vertical salinity stratification, this significant change in the magnitude of the diffusive term in the BG is indicative of a change in the vertical salinity stratification over this region (Davis et al., 2016). In the ESS, the vertical integral of  $VAR_{dif}$  is a sink almost everywhere over the two periods and undergoes a small decrease in amplitude in the second period (−14%, Table 2).

## 6. Conclusion

In this paper, we have used for the first time a salinity variance budget to investigate the mechanisms responsible for the interannual variations of salinity in the Arctic in a realistic framework. This methodology allows to test the main hypotheses of the BG variability, previously established using idealized configurations of simple models, and to extend the study area to the entire Arctic. Using the ECCO v4r3 state estimate, we quantify, for the first time, the main sources and sinks of salinity variability in the Arctic.

The main source of salinity variability is due to the salinity flux associated with the interannual circulation across mean salinity surfaces which are very close to isopycnal surfaces in a  $\beta$  ocean. This term can also be interpreted as a salinity variance transfer between the mean circulation and the interannual salinity variance reservoir (see Figure 5). A similar term was found to be the main contributor of interannual steric sea level variability (Hochet et al., 2023). Additionally, parameterized eddy fluxes are identified as the primary sink of salinity variance, which is in close balance with the main source. This is confirmed by the spatial average over the Arctic of the individual budget terms (Table 1), which shows that salinity flux across mean salinity surfaces represents 63% of all sources whereas the parametrized eddy fluxes represent 65% of all sinks. In the BG, this balance is even more dominant, with 84% of all sources due to the salinity flux across mean salinity surfaces and 86% to the parametrized eddy fluxes. This result is in agreement with previous results obtained in idealized configurations of the BG showing the importance of the residual circulation framework (e.g., Manucharyan et al., 2016; Spall, 2013).

We also show that, although these two terms are the largest contributors to the budget, other terms are not negligible. Fluctuating surface freshwater fluxes (mainly due to sea ice formation/melting) are almost everywhere a source of interannual salinity variations whereas the diffusive terms in the interior are a sink. When averaged over the Arctic Basin, they contribute for 25% of all sources and 24% of all sinks of variability, respectively (Table 1). Over the ESS, where large level of interannual salinity variance are found (Figure 2), the main source is associated to fluctuating surface freshwater fluxes (61% of all sources) and the sink to a combination of parameterized eddy fluxes (46%) and diffusive terms (27%). Our results also confirm that the main source term of interannual salinity variations in the BG (i.e., the advection of interannual salinity anomalies in the direction opposite to the mean salinity gradient) appears to be sustained by wind variations via Ekman pumping. The transmission of the wind stress to the ocean in the deep basins is mediated, for approximately 60%, by the ice-ocean stress where sea ice is present, and for 40% directly to the ocean where there is no sea ice. Because of the important on-going sea ice decline (Meredith et al., 2019), it is expected that the part linked with the ice-ocean stress will decrease in the coming decades and that the part linked with the direct wind-ocean stress will increase. This has the potential to significantly alter the BG dynamic as the presence of sea-ice provides an attenuation mechanisms for the gyre via the “ice-ocean stress governor” (Meneghello et al., 2018). In addition, modifications in the subarctic inflows to the Arctic have been shown to cause significant changes in the properties of the Arctic water masses (A. Woodgate & Peralta-Ferriz, 2021). Therefore, future studies should consider decomposing the salinity variance convergence term (e.g.,  $VAR_{adv}^{adv}$ ) into different inflow components (e.g., Fram Strait, Davis Strait, Bering Strait, Barents Sea Opening) to better understand their effects on Arctic dynamics. In the ESS, the dynamics of interannual salinity variations are different from those in the BG. In fact, the ESS variations are mainly driven by freshwater fluxes associated with sea ice melting and freezing (61% of all sources), while the sinks are associated with the eddy flux term (46% of all sinks) and secondly with the diffusive terms (27% of all sinks). The fact that the dynamics of the ESS are quite different from those of the BG is not surprising, since the latter is a deep-water gyre and the former is a shelf region affected by river runoff, different winds, and a distinct variability in sea ice.

The intensity of the BG is known to have changed over the studied period (1993–2014) (Armitage et al., 2017; Regan et al., 2019) because of an intensification of the anticyclonic conditions over the Beaufort Sea (Armitage et al., 2017). In our results it is apparent from the averaged salinity variance for the period 1993–2003 and 2004–

2014 (Figure 6) that the salinity variability in the BG has increased in the most recent period. This increase goes together with an increased salinity flux in the direction opposite to the mean salinity gradient that is associated to an increase in Ekman pumping variation. This increased source of variability is balanced by a larger sink associated with parameterized eddy fluxes. Beyond the BG, an opposite dynamical change is also visible in the ESS with a decrease of salinity variance sources and sinks over the most recent 2004–2014 period compared to the 1993–2003 period. We speculate that these opposite variations in the BG and in the ESS are the consequence of the complex imprint of the Arctic Oscillation on the Arctic Ocean as shown in Morison et al. (2021).

The main limitation of our study is the use of a laminar model where mesoscale eddies are not explicitly resolved and thus parameterized by means of a GM scheme. Mesoscale eddies are indeed ubiquitous in the Arctic (Carpenter & Timmermans, 2012; Kubryakov et al., 2021; Manley & Hunkins, 1985; Spall et al., 2008; Zhao et al., 2014). Analysis of high resolution models outputs (Regan et al., 2020; Q. Wang et al., 2020) reveals that most of the eddy kinetic energy (EKE) is located along the continental slope and potentially associated to the destabilization of slope jets as described by Spall et al. (2008). Moreover, using a high resolution simulation, Regan et al. report that EKE did not increase in response to gyre spin-up associated to increased anticyclonic conditions in 2007. They suggest that this is in apparent contradiction with the main theories of the gyre mechanisms which find that an increased Ekman pumping is balanced by an increased eddy flux of opposite sign and should thus be associated to an increased EKE. On the contrary, in ECCO, the effect of the parameterized eddy induced salt flux, which acts as a sink of salinity variance, is located approximately in the same region as the source associated with fluctuating winds (Figures 3a and 3b), and increases when the Ekman pumping increases, in agreement with the literature. One hypothesis could be that laminar models (such as the ECCO V4r3) are unable to correctly represent the BG dynamic obtained in eddy-resolving simulations (Manucharyan et al., 2017). However, how the variations in EKE and the variations in eddy induced salt flux should relate is not completely clear. We have shown in Section 4.4 that previous development based on the residual mean theories can be linked to the salinity variance budget. It thus seems natural to assess these theoretical hypotheses using salinity variance budget. In contrast, the link between these theoretical hypotheses and kinetic energy budget is less clear. Therefore future investigations should focus on computing both salinity variance budget and kinetic energy budget in high-resolution simulations in order to clarify these questions. Another important limitation is associated to the use of climatological runoff in ECCO. It is well established that Arctic river discharge changes on interannual time scales, either due to atmospheric interannual variability (Morison et al., 2012) or to a long-term trend associated with climate change (Feng et al., 2021; Shiklomanov et al., 2021). Thus, a potentially important term is missing from the salinity variance budget, and future studies should account for this effect.

To conclude, we believe that the salinity variance budget applied here to the Arctic Ocean offers a new point of view on the mechanisms of interannual salinity variability and we hope that it will contribute to a better understanding of the Arctic dynamics. A major advantage of the methodology developed in this article is that these variance budgets are relatively simple to compute and theoretically robust. They could be very helpful to compare and assess the mechanisms of interannual variability in different numerical models (including coupled climate models) as well as in observations. Moreover, the same methodology could be used to study the mechanisms of salinity variations on different timescales such as the drivers of seasonal variations of salinity and to study the effect of climate change on the mechanisms of salinity variations.

### Appendix A: Interpretation of $\text{VAR}_{\text{adv}}^{\text{mean}}$ and $\text{VAR}_{\text{adv}}^{\text{eddy}}$ as Transfers of Variance Between the Mean and Interannual Circulations

The equation for the time mean salinity is:

$$\frac{\partial \bar{S}}{\partial t} = \overline{\text{adv}} + \overline{\text{dif}} + \overline{\text{flu}}, \quad (\text{A1})$$

Multiplying this equation by the time mean salinity  $\bar{S}$  gives the equation for the square time-mean salinity:

$$\frac{1}{2} \frac{\partial \bar{S}^2}{\partial t} = \bar{S} \overline{\text{adv}} + \bar{S} \overline{\text{dif}} + \bar{S} \overline{\text{flu}}. \quad (\text{A2})$$

in this equation, the advective terms  $\overline{\bar{S}} \overline{\text{adv}}$  can be decomposed as follows:

$$\overline{\bar{S}} \overline{\text{adv}} = -\frac{1}{2} \nabla \cdot (\overline{\mathbf{v} + \mathbf{v}_{GM}} \overline{S^2}) - \overline{\bar{S}} \nabla \cdot \overline{\mathbf{v}' S'} - \overline{\bar{S}} \nabla \cdot \overline{\mathbf{v}'_{GM} S'} - \overline{\text{adv}_{\text{sub}}}, \quad (\text{A3})$$

where the first term on the r.h.s. is the local convergence of variance due to both the mean resolved and parametrized eddy induced velocities, the second and third terms represent the effect of interannual frequencies, the last term the effect of resolved sub-annual frequencies. The second and third terms (i.e.,  $-\overline{\bar{S}} \nabla \cdot \overline{\mathbf{v}' S'}$  and  $-\overline{\bar{S}} \nabla \cdot \overline{\mathbf{v}'_{GM} S'}$ ) are further decomposed into two terms:

$$\begin{aligned} -\overline{\bar{S}} \nabla \cdot \overline{\mathbf{v}' S'} &= -\nabla \cdot (\overline{\bar{S}} \overline{\mathbf{v}' S'}) + \underbrace{\overline{\mathbf{v}' S'} \cdot \nabla \overline{\bar{S}}}_{= -\text{VAR}_{\text{adv}}^{\text{mean}}}, \\ -\overline{\bar{S}} \nabla \cdot \overline{\mathbf{v}'_{GM} S'} &= -\nabla \cdot (\overline{\bar{S}} \overline{\mathbf{v}'_{GM} S'}) + \underbrace{\overline{\mathbf{v}'_{GM} S'} \cdot \nabla \overline{\bar{S}}}_{= -\text{VAR}_{\text{adv}}^{\text{eddy}}}. \end{aligned}$$

The first term in the r.h.s of the two equations is a divergence term associated to non-local transfer of variance between the mean and interannual circulations. A similar term has been studied in the context of kinetic energy transfers (e.g., Chen et al., 2014; Chen et al., 2016; Jamet et al., 2022, and references therein). This term disappears when integrated over the volume of the ocean, so it cannot be a global net source or sink of variance but a non-local redistribution. The second term in the r.h.s of each line are the opposite of the term  $\text{VAR}_{\text{adv}}^{\text{mean}}$  and  $\text{VAR}_{\text{adv}}^{\text{eddy}}$  for the first and second line, respectively. It therefore demonstrates that  $\text{VAR}_{\text{adv}}^{\text{mean}}$  and  $\text{VAR}_{\text{adv}}^{\text{eddy}}$  can be interpreted as a variance transfer between the time-mean and interannual circulations.

## Data Availability Statement

This study uses ECCO v4r3 which can be found here: <https://ecco-group.org/products.htm>. The PHC 3.0 climatology can be downloaded here: [http://psc.apl.washington.edu/nonwp\\_projects/PHC/](http://psc.apl.washington.edu/nonwp_projects/PHC/) and the CCI Sea ice dataset on the copernicus data store website: <https://cds.climate.copernicus.eu/>.

## Acknowledgments

ECCO v4r3 salinity budget computations were greatly facilitated by the existence of the `ecco_v4_py` Python library, and by several tutorials which can be found at: <https://ecco-v4-python-tutorial.readthedocs.io/>. We warmly acknowledge the authors of this work. AH is supported by an ESA living planet fellowship under the PACIFIC project. AH and FS are supported by the ARVOR project funded through the French CNRS/INSU/LEFE program. FS and CL are supported by the CLIMArctic project funded by the ‘‘PPR Océan et Climat—France 2030’’ (contrat ANR-22-POCE-0005). FS and WL are supported by the EERIE project (Grant Agreement 101081383) funded by the European Union. We thank two anonymous reviewers for their constructive comments, which helped us to improve an earlier version of the manuscript.

## References

- Aagaard, K., & Carmack, E. C. (1989). The role of sea ice and other fresh water in the Arctic circulation. *Journal of Geophysical Research*, 94(C10), 14485–14498. <https://doi.org/10.1029/JC094iC10p14485>
- Antonov, J. I., Seidov, D., Boyer, T. P., Locarnini, R. A., Mishonov, A. V., Garcia, H. E., et al. (2010). World ocean Atlas 2009. *Salinity*, 2.
- Armitage, T. W., Bacon, S., Ridout, A. L., Petty, A. A., Wolbach, S., & Tsamados, M. (2017). Arctic Ocean surface geostrophic circulation 2003–2014. *The Cryosphere*, 11(4), 1767–1780. <https://doi.org/10.5194/tc-11-1767-2017>
- Arzel, O., Huck, T., & Colin de Verdière, A. (2006). The different nature of the interdecadal variability of the thermohaline circulation under mixed and flux boundary conditions. *Journal of Physical Oceanography*, 36(9), 1703–1718. <https://doi.org/10.1175/jpo2938.1>
- Arzel, O., Huck, T., & Colin de Verdière, A. (2018). The internal generation of the Atlantic Ocean interdecadal variability. *Journal of Climate*, 31(16), 6411–6432. <https://doi.org/10.1175/jcli-d-17-0884.1>
- Bulgakov, N. (1962). The role of convection in the mechanism of heat transfer of deep Atlantic water. *Deep-Sea Research and Oceanographic Abstracts*, 9(5), 233–239. [https://doi.org/10.1016/0011-7471\(62\)90176-6](https://doi.org/10.1016/0011-7471(62)90176-6)
- Carmack, E. C. (2007). The alpha/beta ocean distinction: A perspective on freshwater fluxes, convection, nutrients and productivity in high-latitude seas. *Deep Sea Research Part II: Topical Studies in Oceanography*, 54(23), 2578–2598. <https://doi.org/10.1016/j.dsr2.2007.08.018>
- Carpenter, J. R., & Timmermans, M.-L. (2012). Deep mesoscale eddies in the Canada basin, Arctic Ocean. *Geophysical Research Letters*, 39(20). <https://doi.org/10.1029/2012GL053025>
- Chen, R., Flierl, G. R., & Wunsch, C. (2014). Description of local and nonlocal eddy-mean flow interaction in a global eddy-permitting state estimate. *Journal of Physical Oceanography*, 44(9), 2336–2352. <https://doi.org/10.1175/jpo-d-14-0009.1>
- Chen, R., Thompson, A. F., & Flierl, G. R. (2016). Time-dependent eddy-mean energy diagrams and their application to the Ocean. *Journal of Physical Oceanography*, 46(9), 2827–2850. <https://doi.org/10.1175/jpo-d-16-0012.1>
- Colin de Verdière, A., & Huck, T. (1999). Baroclinic instability: An oceanic wavemaker for interdecadal variability. *Journal of Physical Oceanography*, 29(5), 893–910. [https://doi.org/10.1175/1520-0485\(1999\)029<0893:biaowf>2.0.co;2](https://doi.org/10.1175/1520-0485(1999)029<0893:biaowf>2.0.co;2)
- Dai, A., & Trenberth, K. E. (2002). Estimates of freshwater discharge from continents: Latitudinal and seasonal variations. *Journal of Hydro-meteorology*, 3(6), 660–687. [https://doi.org/10.1175/1525-7541\(2002\)003<0660:eoofdc>2.0.co;2](https://doi.org/10.1175/1525-7541(2002)003<0660:eoofdc>2.0.co;2)
- Davis, P. E. D., Lique, C., & Johnson, H. L. (2014). On the link between Arctic Sea ice decline and the freshwater content of the Beaufort Gyre: Insights from a simple process model. *Journal of Climate*, 27(21), 8170–8184. <https://doi.org/10.1175/JCLI-D-14-00090.1>
- Davis, P. E. D., Lique, C., Johnson, H. L., & Guthrie, J. D. (2016). Competing effects of elevated vertical mixing and increased freshwater input on the stratification and sea ice cover in a changing Arctic Ocean. *Journal of Physical Oceanography*, 46(5), 1531–1553. <https://doi.org/10.1175/JPO-D-15-0174.1>

- Doddridge, E. W., Meneghello, G., Marshall, J., Scott, J., & Lique, C. (2019). A three-way balance in the Beaufort Gyre: The ice-ocean governor, wind stress, and eddy diffusivity. *Journal of Geophysical Research: Oceans*, *124*(5), 3107–3124. <https://doi.org/10.1029/2018JC014897>
- Fekete, B. M., Vörösmarty, C. J., & Grabs, W. (2002). High-resolution fields of global runoff combining observed river discharge and simulated water balances. *Global Biogeochemical Cycles*, *16*(3), 15–21. <https://doi.org/10.1029/1999gb001254>
- Feng, D., Gleason, C. J., Lin, P., Yang, X., Pan, M., & Ishitsuka, Y. (2021). Recent changes to Arctic River discharge. *Nature Communications*, *12*(1), 6917. <https://doi.org/10.1038/s41467-021-27228-1>
- Forget, G., Campin, J.-M., Heimbach, P., Hill, C. N., Ponte, R. M., & Wunsch, C. (2015). ECCO version 4: An integrated framework for non-linear inverse modeling and Global Ocean state estimation [Dataset]. *Geoscientific Model Development*, *8*(10), 3071–3104. <https://doi.org/10.5194/gmd-8-3071-2015>
- Fournier, S., Lee, T., Wang, X., Armitage, T. W. K., Wang, O., Fukumori, I., & Kwok, R. (2020). Sea surface salinity as a proxy for Arctic Ocean freshwater changes. *Journal of Geophysical Research: Oceans*, *125*(7), e2020JC016110. <https://doi.org/10.1029/2020JC016110>
- Fukumori, I., Wang, O., Fenty, I., Forget, G., Heimbach, P., & Ponte, R. M. (2017). ECCO version 4 release 3.
- Gastineau, G., Mignot, J., Arzel, O., & Huck, T. (2018). North Atlantic Ocean internal decadal variability: Role of the mean state and Ocean-Atmosphere coupling. *Journal of Geophysical Research: Oceans*, *123*(8), 5949–5970. <https://doi.org/10.1029/2018jc014074>
- Gent, P. R., & McWilliams, J. C. (1990). Isopycnal mixing in ocean circulation models. *Journal of Physical Oceanography*, *20*(1), 150–155. [https://doi.org/10.1175/1520-0485\(1990\)020<0150:imiocm>2.0.co;2](https://doi.org/10.1175/1520-0485(1990)020<0150:imiocm>2.0.co;2)
- Haine, T. W., Curry, B., Gerdes, R., Hansen, E., Karcher, M., Lee, C., et al. (2015). Arctic freshwater export: Status, mechanisms, and prospects. *Global and Planetary Change*, *125*, 13–35. <https://doi.org/10.1016/j.gloplacha.2014.11.013>
- Häkkinen, S., & Proshutinsky, A. (2004). Freshwater content variability in the Arctic Ocean. *Journal of Geophysical Research: Oceans*, *109*(C3). <https://doi.org/10.1029/2003jc001940>
- Hendricks, S., Paul, S., Rinne, E., Initiative, E. S. I. C. C., et al. (2018). Northern Hemisphere sea ice thickness from the Cryosat-2 satellite on a monthly grid (13c), v2. 0. *Centre for Environmental Data Analysis*.
- Hochet, A., Huck, T., Arzel, O., Sévellec, F., de Verdière, A. C., Mazloff, M., & Cornuelle, B. (2020). Direct temporal cascade of temperature variance in eddy-permitting simulations of multidecadal variability. *Journal of Climate*, *33*(21), 9409–9425. <https://doi.org/10.1175/jcli-d-19-0921.1>
- Hochet, A., Huck, T., & Colin De Verdière, A. (2015). Large-scale baroclinic instability of the mean oceanic circulation: A local approach. *Journal of Physical Oceanography*, *45*(11), 2738–2754. <https://doi.org/10.1175/jpo-d-15-0084.1>
- Hochet, A., Llovel, W., Huck, T., & Sévellec, F. (2024). Advection surface-flux balance controls the seasonal steric sea level amplitude. *Scientific Reports*, *14*(1). <https://doi.org/10.1038/s41598-024-61447-y>
- Hochet, A., Llovel, W., Sévellec, F., & Huck, T. (2023). Sources and sinks of interannual Steric Sea Level variability. *Journal of Geophysical Research: Oceans*, *128*(4). <https://doi.org/10.1029/2022JC019335>
- Holland, M. M., Finnis, J., & Serreze, M. C. (2006). Simulated Arctic Ocean freshwater budgets in the twentieth and twenty-first centuries. *Journal of Climate*, *19*(23), 6221–6242. <https://doi.org/10.1175/jcli3967.1>
- Jahn, A., & Holland, M. M. (2013). Implications of Arctic sea ice changes for North Atlantic deep convection and the meridional overturning circulation in CCSM4-CMIP5 simulations. *Geophysical Research Letters*, *40*(6), 1206–1211. <https://doi.org/10.1002/grl.50183>
- Jahn, A., Sterling, K., Holland, M. M., Kay, J. E., Maslanik, J. A., Bitz, C. M., et al. (2012). Late-twentieth-century simulation of Arctic sea ice and ocean properties in the CCSM4. *Journal of Climate*, *25*(5), 1431–1452. <https://doi.org/10.1175/JCLI-D-11-00201.1>
- Jamet, Q., Leroux, S., Dewar, W. K., Penduff, T., Le Sommer, J., Molines, J.-m., & Gula, J. (2022). Non-local eddy-mean kinetic energy transfers in submesoscale-permitting ensemble simulations. *Journal of Advances in Modeling Earth Systems*, *14*(10). <https://doi.org/10.1029/2022ms003057>
- Johnson, H. L., Cornish, S. B., Kostov, Y., Beer, E., & Lique, C. (2018). Arctic Ocean freshwater content and its decadal memory of sea-level pressure. *Geophysical Research Letters*, *45*(10), 4991–5001. <https://doi.org/10.1029/2017gl076870>
- Karcher, M., Gerdes, R., Kauker, F., Köberle, C., & Yashayaev, I. (2005). Arctic Ocean change heralds North Atlantic freshening. *Geophysical Research Letters*, *32*(21). <https://doi.org/10.1029/2005gl023861>
- Khosravi, N., Wang, Q., Koldunov, N., Hinrichs, C., Semmler, T., Danilov, S., & Jung, T. (2022). The Arctic Ocean in CMIP6 models: Biases and projected changes in temperature and salinity. *Earth's Future*, *10*(2), e2021EF002282. <https://doi.org/10.1029/2021EF002282>
- Köberle, C., & Gerdes, R. (2007). Simulated variability of the Arctic Ocean freshwater balance 1948–2001. *Journal of Physical Oceanography*, *37*(6), 1628–1644. <https://doi.org/10.1175/jpo3063.1>
- Kubryakov, A. A., Kozlov, I. E., & Manucharyan, G. E. (2021). Large mesoscale eddies in the western Arctic Ocean from satellite altimetry measurements. *Journal of Geophysical Research: Oceans*, *126*(5), e2020JC016670. <https://doi.org/10.1029/2020JC016670>
- Lique, C., Garric, G., Treguier, A.-M., Barnier, B., Ferry, N., Testut, C.-E., & Girard-Ardhuin, F. (2011). Evolution of the Arctic Ocean salinity, 2007–08: Contrast between the Canadian and the Eurasian basins. *Journal of Climate*, *24*(6), 1705–1717. <https://doi.org/10.1175/2010JCLI3762.1>
- Lique, C., Treguier, A. M., Scheinert, M., & Penduff, T. (2009). A model-based study of ice and freshwater transport variability along both sides of Greenland. *Climate Dynamics*, *33*(5), 685–705. <https://doi.org/10.1007/s00382-008-0510-7>
- Losch, M., Menemenlis, D., Campin, J.-M., Heimbach, P., & Hill, C. (2010). On the formulation of sea-ice models. Part 1: Effects of different solver implementations and parameterizations. *Ocean Modelling*, *33*(1), 129–144. <https://doi.org/10.1016/j.ocemod.2009.12.008>
- Manley, T. O., & Hunkins, K. (1985). Mesoscale eddies of the Arctic Ocean. *Journal of Geophysical Research: Oceans*, *90*(C3), 4911–4930. <https://doi.org/10.1029/JC090iC03p04911>
- Manucharyan, G. E., & Spall, M. A. (2016). Wind-driven freshwater buildup and release in the Beaufort Gyre constrained by mesoscale eddies. *Geophysical Research Letters*, *43*(1), 273–282. <https://doi.org/10.1002/2015GL065957>
- Manucharyan, G. E., Spall, M. A., & Thompson, A. F. (2016). A theory of the wind-driven Beaufort Gyre variability. *Journal of Physical Oceanography*, *46*(11), 3263–3278. <https://doi.org/10.1175/JPO-D-16-0091.1>
- Manucharyan, G. E., Thompson, A. F., & Spall, M. A. (2017). Eddy memory mode of multidecadal variability in residual-mean ocean circulations with application to the Beaufort Gyre. *Journal of Physical Oceanography*, *47*(4), 855–866. <https://doi.org/10.1175/JPO-D-16-0194.1>
- Marshall, J., & Radko, T. (2003). Residual-mean solutions for the Antarctic Circumpolar Current and its associated overturning circulation. *Journal of Physical Oceanography*, *33*(11), 2341–2354. [https://doi.org/10.1175/1520-0485\(2003\)033<2341:rsftac>2.0.co;2](https://doi.org/10.1175/1520-0485(2003)033<2341:rsftac>2.0.co;2)
- Meneghello, G., Marshall, J., Campin, J.-M., Doddridge, E., & Timmermans, M.-L. (2018). The ice-ocean governor: Ice-ocean stress feedback limits Beaufort Gyre spin-up. *Geophysical Research Letters*, *45*(20), 11–293. <https://doi.org/10.1029/2018gl080171>
- Meneghello, G., Marshall, J., Cole, S. T., & Timmermans, M.-L. (2017). Observational inferences of Lateral eddy diffusivity in the halocline of the Beaufort Gyre. *Geophysical Research Letters*, *44*(24), 331–338. <https://doi.org/10.1002/2017GL075126>

- Meredith, M., Sommerkorn, M., Cassota, S., Derksen, C., Ekaykin, A., Hollowed, A., et al. (2019). Polar regions, In H.-O. Pörtner, D.C. Roberts, V. Masson-Delmotte, P. Zhai, M. Tignor, E. Poloczanska, K. Mintenbeck, A. Alegría, M. Nicolai, A. Okem, J. Petzold, B. Rama, N.M. Weyer (Eds.), *IPCC Special Report on the Ocean and Cryosphere in a Changing Climate*. In press.
- Morison, J., Kwok, R., Dickinson, S., Andersen, R., Peralta-Ferriz, C., Morison, D., et al. (2021). The cyclonic mode of Arctic Ocean circulation. *Journal of Physical Oceanography*, *51*(4), 1053–1075. <https://doi.org/10.1175/JPO-D-20-0190.1>
- Morison, J., Kwok, R., Peralta-Ferriz, C., Alkire, M., Rigor, I., Andersen, R., & Steele, M. (2012). Changing Arctic Ocean freshwater pathways. *Nature*, *481*(7379), 66–70. <https://doi.org/10.1038/nature10705>
- Notz, D., & Community, S. (2020). Arctic sea ice in CMIP6. *Geophysical Research Letters*, *47*(10), e2019GL086749. <https://doi.org/10.1029/2019GL086749>
- Proshutinsky, A., Bourke, R. H., & McLaughlin, F. A. (2002). The role of the Beaufort Gyre in Arctic climate variability: Seasonal to decadal climate scales. *Geophysical Research Letters*, *29*(23), 151–154. <https://doi.org/10.1029/2002GL015847>
- Proshutinsky, A., Krishfield, R., Timmermans, M.-L., Toole, J., Carmack, E., McLaughlin, F., et al. (2009). Beaufort Gyre freshwater reservoir: State and variability from observations. *Journal of Geophysical Research: Oceans*, *114*(C1). <https://doi.org/10.1029/2008JC005104>
- Rabe, B., Karcher, M., Kauker, F., Schauer, U., Toole, J. M., Krishfield, R. A., et al. (2014). Arctic Ocean basin liquid freshwater storage trend 1992–2012. *Geophysical Research Letters*, *41*(3), 961–968. <https://doi.org/10.1002/2013GL058121>
- Regan, H., Lique, C., & Armitage, T. W. K. (2019). The Beaufort Gyre extent, shape, and location between 2003 and 2014 from satellite observations. *Journal of Geophysical Research: Oceans*, *124*(2), 844–862. <https://doi.org/10.1029/2018JC014379>
- Regan, H., Lique, C., Talandier, C., & Meneghello, G. (2020). Response of total and eddy kinetic energy to the recent spinup of the Beaufort Gyre. *Journal of Physical Oceanography*, *50*(3), 575–594. <https://doi.org/10.1175/JPO-D-19-0234.1>
- Serreze, M. C., Barrett, A. P., Slater, A. G., Woodgate, R. A., Aagaard, K., Lammers, R. B., et al. (2006). The large-scale freshwater cycle of the Arctic. *Journal of Geophysical Research: Oceans*, *111*(C11). <https://doi.org/10.1029/2005jc003424>
- Sévellec, F., & Fedorov, A. V. (2016). Amoc sensitivity to surface buoyancy fluxes: Stronger ocean meridional heat transport with a weaker amoc? <https://doi.org/10.1007/s00382-015-2915-4>
- Sévellec, F., Naveira Garabato, A., & Huck, T. (2021). Damping of climate-scale oceanic variability by mesoscale eddy turbulence. *Journal of Physical Oceanography*, *51*(2), 491–503. <https://doi.org/10.1175/jpo-d-20-0141.1>
- Shiklomanov, A., Déry, S., Tretiakov, M., Yang, D., Magritsky, D., Georgiadi, A., & Tang, W. (2021). River freshwater flux to the Arctic Ocean. *Arctic Hydrology, Permafrost and Ecosystems*, 703–738. [https://doi.org/10.1007/978-3-030-50930-9\\_24](https://doi.org/10.1007/978-3-030-50930-9_24)
- Shu, Q., Wang, Q., Song, Z., Qiao, F., Zhao, J., Chu, M., & Li, X. (2020). Assessment of Sea Ice extent in CMIP6 with comparison to observations and CMIP5. *Geophysical Research Letters*, *47*(9), e2020GL087965. <https://doi.org/10.1029/2020GL087965>
- Spall, M. A. (2013). On the circulation of Atlantic water in the Arctic Ocean. *Journal of Physical Oceanography*, *43*(11), 2352–2371. <https://doi.org/10.1175/JPO-D-13-079.1>
- Spall, M. A., Pickart, R. S., Fratantoni, P. S., & Plueddemann, A. J. (2008). Western Arctic shelfbreak eddies: Formation and transport. *Journal of Physical Oceanography*, *38*(8), 1644–1668. <https://doi.org/10.1175/2007jpo3829.1>
- Steele, M., Morley, R., & Ermold, W. (2001). PHC: A global ocean hydrography with a high-quality Arctic Ocean. *Journal of Climate*, *14*(9), 2079–2087. [https://doi.org/10.1175/1520-0442\(2001\)014<2079:pagoHW>2.0.co;2](https://doi.org/10.1175/1520-0442(2001)014<2079:pagoHW>2.0.co;2)
- Steele, M., Thomas, D., Rothrock, D., & Martin, S. (1997). A simple model study of the Arctic Ocean fresh-water balance, 1979–1985. *Oceanographic Literature Review*, *5*(44), 420.
- Stewart, K. D., & Haine, T. W. N. (2013). Wind-driven Arctic freshwater anomalies. *Geophysical Research Letters*, *40*(23), 6196–6201. <https://doi.org/10.1002/2013GL058247>
- Timmermans, M.-L., & Marshall, J. (2020). Understanding Arctic Ocean circulation: A review of Ocean dynamics in a changing climate. *Journal of Geophysical Research: Oceans*, *125*(4), e2018JC014378. <https://doi.org/10.1029/2018JC014378>
- Timmermans, M.-L., & Toole, J. M. (2023). The Arctic Ocean's Beaufort Gyre. *Annual Review of Marine Science*, *15*(1), 223–248. <https://doi.org/10.1146/annurev-marine-032122-012034>
- Toole, J. M., Krishfield, R. A., Timmermans, M.-L., & Proshutinsky, A. (2011). The ice-tethered profiler: Argo of the Arctic. *Oceanography*, *24*(3), 126–135. <https://doi.org/10.5670/oceanog.2011.64>
- Tsubouchi, T., Bacon, S., Aksenov, Y., Garabato, A. C. N., Beszczynska-Möller, A., Hansen, E., et al. (2018). The Arctic Ocean seasonal cycles of heat and freshwater fluxes: Observation-based inverse estimates. *Journal of Physical Oceanography*, *48*(9), 2029–2055. <https://doi.org/10.1175/JPO-D-17-0239.1>
- Wang, H., Legg, S., & Hallberg, R. (2018). The effect of Arctic freshwater pathways on North Atlantic convection and the Atlantic meridional overturning circulation. *Journal of Climate*, *31*(13), 5165–5188. <https://doi.org/10.1175/jcli-d-17-0629.1>
- Wang, Q., Ilicak, M., Gerdes, R., Drange, H., Aksenov, Y., Bailey, D. A., et al. (2016). An assessment of the Arctic Ocean in a suite of interannual CORE-II simulations. Part II: Liquid freshwater. *Ocean Modelling*, *99*, 86–109. <https://doi.org/10.1016/j.ocemod.2015.12.009>
- Wang, Q., Koldunov, N. V., Danilov, S., Sidorenko, D., Wekerle, C., Scholz, P., et al. (2020). Eddy kinetic energy in the Arctic Ocean from a Global simulation with a 1-km Arctic. *Geophysical Research Letters*, *47*(14). <https://doi.org/10.1029/2020GL088550>
- Woodgate, A. R., & Peralta-Ferriz, C. (2021). Warming and freshening of the Pacific inflow to the arctic from 1990–2019 implying dramatic shoaling in Pacific winter water ventilation of the Arctic water column. *Geophysical Research Letters*, *48*(9), e2021GL092528. <https://doi.org/10.1029/2021GL092528>
- Yang, J., Proshutinsky, A., & Lin, X. (2016). Dynamics of an idealized Beaufort Gyre: 1. The effect of a small beta and lack of western boundaries. *Journal of Geophysical Research: Oceans*, *121*(2), 1249–1261. <https://doi.org/10.1002/2015JC011296>
- Zhao, M., Timmermans, M.-L., Cole, S., Krishfield, R., Proshutinsky, A., & Toole, J. (2014). Characterizing the eddy field in the Arctic Ocean halocline. *Journal of Geophysical Research: Oceans*, *119*(12), 8800–8817. <https://doi.org/10.1002/2014JC010488>